AD-A259 586

AFIT/GCS/ENG/92D-21

Scientific Visualization of Volumetric
Radar Cross Section Data

THESIS

Thomas G. Wojszynski
Captain, USAF

AFIT/GCS/ENG/92D-21

DTIC
S ELECTE D
JAN 0 7 1993
E

93-00107

93   1 04 153

Scientific Visualization

of

Volumetric Radar Cross Section Data

THESIS

Presented to the Faculty of the School of Engineering

of the Air Force Institute of Technology

Air University

In Partial Fulfillment of the

Requirements for the Degree of

Master of Science in Electrical Engineering

Thomas George Wojszynski, B.S.E.E.

Captain, USAF

December, 1992

Accesion For		
NTIS CRA&I		☒
DTIC TAB		☐
Unannounced		☐
Justification		
By		
Distribution /		
Availability Codes		
Dist	Avail and / or Special	
A-1		

Approved for public release; distribution unlimited

DTIC QUALITY INSPECTED 1

Table of Contents

iv

List of Figures

List of Tables

AFIT/GCS/ENG/92D-21

Abstract

For aircraft design and mission planning, designers, threat analysts, mission planners, and pilots require a Radar Cross Section (RCS) central tendency with its associated distribution about a specified aspect and its relation to a known threat. Historically, RCS data sets have been statically analyzed to evaluate a design or mission profile. However, Scientific Visualization, the application of computer graphics techniques to produce pictures of complex physical phenomena, appears to be a more promising tool to interpret this data. This work describes data reduction techniques and a surface rendering algorithm to construct and display a complex polyhedron from adjacent contours of RCS data. Data reduction is accomplished by sectorizing the data and characterizing the statistical properties of the data. Color, lighting, and orientation cues are added to complete the visualization system. The tool may be useful for synthesis, design, and analysis of complex, low observable air vehicles.

Scientific Visualization

of

Volumetric Radar Cross Section Data

I. Introduction

1.1 Background

The first thing one notices about stealth, or low-observable (LO), aircraft is their shape. The F-117A's unique faceted shape allowed aircraft designers to minimize enemy radar's reflectivity and maximize the survivability of the aircraft, and more importantly, the pilot. In 1991, the undisputed success of the F-117A during the Gulf War proved the value of stealth. In fact, according to Gen Loh, Commander, Air Combat Command, future fighters must combine low observability and speed to achieve a first-look, first-shot capability in tomorrow's battles (30).

To meet these future requirements, air vehicle [1] designers work with electrical engineers and members of other disciplines to balance aerodynamic performance with low-observability. Several factors contribute to an air vehicle's total observability, but the primary component in today's electromagnetic threat environment is the *radar signature*, or Radar Cross Section (RCS). Although many mathematically rigorous definitions of RCS exist, Sweetman (43) provides a more intuitive definition: RCS is determined by measuring the reflected radar energy of a target from a given aspect angle, then calculating the size of a reflective sphere that returns an equal amount of energy. The cross-sectional area of the sphere is the target's RCS. The goal for the designer, then, is to achieve low observability by minimizing RCS. To reach this goal, a designer may change the vehicle's shape, construct the vehicle using advanced composites, or apply radar absorbing material to the

---

[1] Air vehicle is used to describe any airborne platform including fixed-wing aircraft, rotary-wing aircraft, and missiles.

skin of the vehicle. Each incremental design change requires the electrical engineer to calculate a new RCS and determine the components contributing to large values of RCS. The designer and engineer continue to further refine the air vehicle design until an effective balance between reduced RCS and aerodynamics is achieved.

Once the air vehicle is operational, threat analysts, mission planners, and pilots require knowledge of the air vehicle's Radar Cross Section (RCS) with its associated statistical distribution about a specified aspect angle and its relation to a known threat. This information is combined with mission objectives, terrain and weather data, intelligence data, and exclusion zone information to plan the most effective mission route to and from a target area (3).

Historically, electrical engineers predicted or measured the RCS at a fixed elevation angle, usually 90°, or waterline, and at a series of azimuthal angles, usually $0 - 360^\circ$, then portrayed the data on two-dimensional (2D) polar plots. Depending on the availability of resources, the prediction or measurement technique was repeated at several elevation angles to provide a representative RCS. Today, with the improvement in both prediction and measurement techniques, RCS data is collected at finer degrees of elevation. Electrical engineers, air vehicle designers, and mission analysts are now faced with a new problem: How does one interpret the large volumes of data? One approach is to mentally piece together the 2D information to create a three-dimensional (3D) impression of the air vehicle's full RCS. Another more promising approach is known as Scientific Visualization—the application of computer graphics techniques to view complex physical properties (20).

Ideally, an interactive visualization tool capable of satisfying the requirements of the engineer, the designer, and the pilc ·ission analyst is needed–this is the domain of the computer engineer specializing in comput r graphics. However, a knowledge of RCS prediction and measurement techniques, data filtering techniques, and the capabilities and limitations of these techniques is necessary for determining the requirements of such a system.

1.2 Problem

Considering the computer graphics techniques available for interactively viewing volumetric RCS data such as volume, surface, and particle systems rendering, the problem is reduced to determining what technique can best portray the necessary information to the user. The high bandwidth of the human visual system can then be used to enhance air vehicle design and mission effectiveness through better understanding of the interactions between the aircraft's RCS and an enemy's threat radars. This work presents a visualization tool using a surface rendering technique that constructs a polygonal model of the 3D RCS and renders the resulting model in an interactive display environment.

1.3 Research Objectives

The main thrust of this work is to apply a surface generation technique that extracts a 3D surface from a volumetric RCS data set and constructs a representative model. Color, lighting, and orientation cues are combined with the resulting model and rendered in an interactive RCS visualization environment. Data filtering techniques are applied to the original data to achieve two sub-objectives. First, because rendering speed is proportional to the number of surfaces rendered, techniques are investigated that limit the data set by extracting the largest value of RCS over a small window of data. Second, because radar engagements are often modeled using statistical properties of the RCS, the data set is reduced by extracting key characteristics such as mean, median and variance over a sector of data then visualizing the resulting statistics.

1.4 Materials and Equipment

To best support this research effort, a basic program development and visualization environment is assumed. The programming environment should be available for developing the necessary code used to construct the 3D model from the data set and should include tools like a compiler

and interactive debugger. The visualization environment should consist of hardware capable of implementing a Z-buffer rendering algorithm for hidden-surface removal, Gouraud shading for color interpolation, and an optimized graphics pipeline for quickly displaying polygonal surfaces. Also, the visualization environment should have a suite of software tools capable of interactively rotating, scaling, and translating complex geometry. These tools should be easily extensible for enhancing the interactive environment.

The tools described are available in the Air Force Institute of Technology's (AFIT) Advanced Interactive Graphics Lab. The lab contains four Silicon Graphics Iris-4D 440/VGXTs with a graphics development environment. The lab also contains two software tools available for this work. The first, The Interactive Satellite Modeler, is a concurrent thesis effort by Pond (36). The second tool is The Advanced Visualizer, a commercially available product developed by Wavefront Technologies (4).

Finally, a key component to this research is the availability of a representative, unclassified, volumetric RCS data set. The Ohio State University, ElectroScience Laboratory, provided the data set for for this research effort

1.5 Scope and Assumptions

The primary goal of this thesis is to develop a visualization tool capable of interactively displaying volumetric RCS data. Several techniques can be applied to this problem: volume visualization, surface rendering, and particle systems. Since these techniques differ widely in their implementation, this thesis concentrated only on surface rendering techniques. Tisdale studied volume visualization and particle systems visualization of RCS data (51).

Techniques used to collect RCS data differ as widely as visualization techniques. Because this effort concentrates on the visualization of the data, it is only important to understand the various techniques used to collect the data, not the underlying physics. The data is assumed to be correct.

4

1.6 Approach

Before visualizing volumetric RCS data, it is important to understand the benefits and limitations of RCS prediction and measurement techniques. This understanding provides the basis for determining the best method to visually display the data and for determining the requirements for data filtering.

Next, investigating and determining an effective polygonal modeling technique on an adjacent pair of 2D data sets is approached. The adjacent slices are connected to form a polyhedron and displayed on the visualization system. Once verified, the technique is applied to the entire data set and modified to work correctly at the boundaries of the data set. Color and orientation cues are added to the environment to complete the visualization system.

After successfully rendering the raw data set using the visualization system, the next step is to apply data filtering techniques to improve the rendering speed of the system and determine statistical characteristics over a sector of data. The reduced data sets are then rendered using the visualization system.

1.7 Summary

This work covers two main areas of research, the necessary background information required to design and implement a RCS visualization system and the results of implementing such a system. The background in Chapters II-III provides information on prediction and measurement techniques used for collection of RCS data, a brief background on data filtering, and a section on computer graphics visualization techniques. Based on this background, Chapter IV details the requirements, design, and implementation issues associated with implementing the visualization system. The results are described in Chapter V along with an interpretation of those results. Finally, Chapter VI presents conclusions and recommendations for future research.

II. Fundamentals of Radar Cross Section

2.1 Introduction

Although this thesis is limited to visualizing RCS data, it is still necessary to understand the origin, processing, and use of volumetric RCS data. This chapter addresses several aspects of RCS data by defining RCS, presenting the current prediction and measurement techniques used to collect RCS, and a summary of current approaches used to filter the data. Because this is an introductory chapter, the discussion is presented with a minimum of mathematics and underlying physics and instead focuses on the importance of RCS in the design and operation of air vehicles.

2.2 Definition of Radar Cross Section

The governing laws of electromagnetism (EM) are a recent discovery. In the late 19th century, Coulomb, Faraday, Ampere, Hertz, and Maxwell determined many of these laws, but it was Maxwell who assembled the results of the early experimenters and formed the basis for modern EM theory. His four equations bear the same relationship to EM that Newton's laws of motion do to classical mechanics. They are the foundation of modern EM principles and explain the theory behind calculation of RCS.

Calculation of RCS is accomplished by analyzing the scattering of an electromagnetic wave as it strikes the boundary of a target. An incident EM wave induces currents on the inside and surface of target. These currents then radiate a scattered EM field. Balanis (6) defines RCS or *echoing area* as the area intercepting that amount of power which, when scattered isotropically, produces at the receiver a density which is equal to that scattered by the actual target. Turner (53) provides a more intuitive definition by stating that RCS is a *measure* of how *strong* the far-scattered fields are for a given illumination . Because RCS is a ratio between the incident and scattered power, it is important to describe the relationship between the direction of the incident power and the direction of scattered power. *Bistatic scattering* is the phrase used to describe the scattering when

the receiver is not collocated with the transmitter, and *monostatic scattering* is the phrase used when source and receiver are collocated (7). In either case, the symbol (σ) is used to represent RCS.

When transmitting and receiving radars are collocated, RCS in equation form is

$$\sigma = 4\pi \lim_{R \to \infty} R^2 \frac{|E^s|^2}{|E^i|^2} \tag{1}$$

where R is the distance from the radar to the target, and E^i and E^s are the incident and scattered electric fields, respectively. The incident field, E^i, is assumed to be a plane wave and contains a dependence on the wavelength (λ). The limit of E^s as $R \to \infty$ ensures the true far-field value of σ is measured since $E^s \sim \frac{1}{R}$ as $R \to \infty$.

Radar Cross Section is usually expressed in units of meters squared (m^2) or in logarithmic form as dB relative to a square meter,

$$\sigma_{dB_{sm}} = 10 \log_{10} \sigma \tag{2}$$

Polarization of the incident and scattered wave also plays a role in determining RCS. The RCS of a rotationally symmetric target like a sphere does not depend on the polarization of the wave, but asymmetrical targets with complex geometries have cross sections that depend on polarization. When describing polarization of RCS, it is customary to describe the properties of the target in terms of its response to horizontally and vertically polarized transmitted waves and is denoted σ_{ij} where i and j represent polarization of the incident and scattered wave, respectively. For example, if the transmitting and receiving antennas are horizontally polarized, the RCS is denoted σ_{HH}. Similarly, if the transmitting antenna is horizontally polarized and the receiving antenna is vertically polarized, the RCS is denoted σ_{HV}.

7

Accurate determination of RCS of real targets with complex geometries is difficult. The frequency, polarization, and phase of the incident wave, and the target's size, shape, and electrical properties all contribute to variations in the magnitude of RCS, but the largest contributor to variations in RCS magnitude is the aspect angle of the incident wave. Each incremental aspect angle presents a different effective area to the incident wave and corresponds to a change in RCS magnitude. For example, in the case of the air vehicle shown in Figure 1, large values of RCS are observed at or near broadside caused by the specular reflection from the side of the fuselage. At other angles, virtual nulls are observed from smaller effective areas and mutual phase cancellation by scattering for different aircraft components (7).

The importance of correctly determining an air vehicle's RCS can be shown by examining the relationship between the maximum detection range of a radar (R_{max}) and σ. The equation for R_{max}, known as the *radar range equation*, is

$$R_{max} = [\frac{P_t G_t G_r \sigma \lambda^2 F_t^2 F_r^2}{(4\pi)^3 (S/N)_{min} k T_s B_n L}]^{\frac{1}{4}} \qquad (3)$$

P_t — Transmitted signal power

G_t — Transmitter power gain

G_r — Receiver power gain

σ — Radar cross section

λ — Wavelength

F_t — Pattern propagation factor for radar to target path

F_r — Pattern propagation factor for target to radar path

S/N_{min} — Minimum Signal-to-Noise ratio for detection

k — Boltzmann's Constant ($1.38 \times 10^{-23} watt - sec/^\circ K$)

T_s — Thermal noise temperature

B_n — Noise bandwidth of the receiver filter

L –   System loss factor

The Radar Range Equation demonstrates why an air vehicle designer strives to reduce RCS. A reduction in RCS has the same effect as minimizing other components in the numerator such as antenna gain, that is $R_{max} \propto \sigma^{\frac{1}{4}}$. For example, suppose a radar detects a 1.0 m^2 target at a distance of 50.0 NM. If the designer can reduce the RCS of the target to 0.001 m^2 ($-30dB_{sm}$), under identical conditions the same radar now detects the target at 8.9 NM.

The methodology for reducing RCS of an air vehicle is a subject in itself and includes techniques such as changing shape, using advanced composites, and applying special radar absorbing material to the skin of the air vehicle (27) (9) (48). The designer is not free to merely minimize the RCS. The designer must balance reduction of RCS with other air vehicle requirements such as aerodynamics, maximum payload, air vehicle mission, etc.

Similarly, it is apparent why the operator of an air vehicle requires detailed information about RCS. If the operator knows the location of threat radars, the operating frequencies of those radars and the corresponding RCS of his air vehicle, he could plan the most survivable mission profile through the threat region by minimizing the detection range (R_{max}) of the threat radars (3). This approach in determining mission routes is used by LO air vehicles like the F-117 and B-2, and will be used by future-generation air vehicles (3).

2.3 RCS Prediction and Measurement Techniques

Traditionally, RCS prediction has been based on detailed inspection of the target geometry by an experienced analyst who would use comparison of similar known targets, identification of features likely to give rise to high returns, and quantitative analysis of these features. This type of expert assessment will continue, but modern techniques provide a more systematic approach to RCS estimation (28). These techniques are

1. Calculations of the approximate solutions of Maxwell's equations on a computer.

2. Static measurements in an anechoic chamber or outdoor range.

3. Dynamic measurements.

Each of these techniques are also subjects in themselves. For the purposes of this work, it is only important to outline the various techniques and their relative advantages and disadvantages. Each technique is presented in order of increasing cost and decreasing ability to repeat the conditions of data generation.

2.3.1 Prediction Techniques Considerable work has been done to predict RCS of simple targets with excellent results; however, the problem is nearly intractable for complex targets such as military platforms. These targets are often composed of thousands of individual scatterers combining to make a total RCS for a given aspect angle. Various methods are used to predict RCS including geometric optics (GO), physical optics (PO), physical theory of diffraction (PTD) and uniform theory of diffraction (UTD). For a thorough discussion of these methods, see Knott, et al. (27). Many of these theories, however, are not applicable to today's anisotropic targets. Newer methods of calculation such as finite-volume time domain methods (FVTD), method of moments (MOM), and finite element methods running on massively parallel multiple-instruction, multiple-data (MIMD) computers continue to refine the process of accurate RCS prediction.

Today, aircraft designers predict RCS by using a computer-aided design (CAD) representation of the target as an input to an RCS prediction program. One such program approximates the RCS by separately computing the cross section of individual scattering elements and adding their contributions to the total RCS. Although this process has historically been time-consuming, advances in computer hardware now make this technique very cost-effective. For example, according to Andersh (5),researchers at Sandia National Laboratories can calculate the single-frequency, single-bounce, 4π steradian RCS of a complex target in 16 minutes using an Intel Hypercube. Mas-

sively parallel computers such as Wavetracer's Data Transport Computer show great promise in bringing these times down to near-interactive rates (23).

2.3.2 Static Measurement Techniques In addition to predicting RCS using computer models, several government agencies and private industries operate indoor anechoic chambers and outdoor radar scattering ranges to measure the "static" RCS. One such range is the U.S. Air Force's Radar Target Scatter (RATSCAT) Range at Holloman Air Force Base, New Mexico (1). The range is equipped with a family of radars operating over several frequency bands, a recording system for collecting results, a rotating target pedestal, and an electromagnetically absorbent background environment. At these indoor and outdoor ranges, full-size or scale models are placed on the rotating pedestal and illuminated with radars operating at varying frequencies. The recording system then collects the data for real-time analysis, or more commonly, for post-processing.

The primary advantage of collecting static RCS data is that it verifies the capability of the prediction technique and compensates for those areas not well-modeled using prediction algorithms. Although computer prediction codes are well-refined, several problem areas like engine inlets and exhaust ducts are difficult to model using CAD packages.

The disadvantage to static collection techniques is the cost associated with the measurement. A separate scale model is normally required for indoor range calculations because most indoor ranges are not equipped to handle full-scale models. Outdoor ranges require special equipment to hoist and mount the vehicles onto the pedestal and extensive precision equipment to accurately measure and collect the data.

2.3.3 Dynamic Measurement Techniques If an aircraft such as the one shown in Figure 1 is in motion, it is apparent that the magnitude of the RCS for a particular aspect angle fluctuates as a function of time. Air vehicles are subject to many changes as they move through the atmosphere such as variations in translational or rotational attitude, aeroelastic effects, and variations in the

11

electromagnetic environment. In order to describe these fluctuations, the ensemble RCS is modeled as probability density function (PDF), or $p(\sigma)$. If σ_{min} is the minimum detectable target cross section at a particular range (R_{max}), then, ignoring receiver noise, the *Probability of Detection* (P_d) is

$$P_d = \int_{\sigma_{min}}^{\infty} p(\sigma)d\sigma \qquad (4)$$

Swerling (44), Weinstock, and others have proposed several PDFs to describe RCS fluctuation statistics. These models include the chi-square family, the Rice family, the Swerling family, and log-normal. Many of these models are based on approximately matching empirical data to known PDFs, because no general method of determining target fluctuation statistics exists.

Two techniques are used to determine dynamic RCS data, each with inherent advantages and disadvantages.

The first technique statistically characterizes the predicted or static data. This approach is relatively cost-effective because a computer can extract the characteristic data and empirically match the data to a known PDF. The disadvantage to this approach is the potential error associated with the underlying static or predicted data.

The second technique uses specially instrumented dynamic measurement ranges to to collect the RCS data. This is the most accurate technique used to represent the relationship between RCS vs. time. It is also the most expensive data collection technique because the measurement system must collect not only the RCS data, but precise information concerning the attitude and speed of the target at the time of illumination. Additionally, the test conditions for this technique are the most difficult to repeat.

2.4 Data Reduction Techniques

Both prediction and measurement techniques produce large amounts of raw data. A typical technique will sweep $0 - 360°$ in azimuth at $0.1°$ resolution, however, this is valid for only one

elevation angle, typically 90°, at one frequency. With emphasis on the design of low observable (LO) air vehicles, designers are collecting RCS data at finer elevation angles and at multiple frequencies. For example, a single-frequency, 4π steradian raw data set can easily consist of 300,000 data points. The number of data points multiplied by the number of frequencies commonly needed during the design phase of an air vehicle makes the total number of data points unwieldy. As researchers collect more raw data, methods for data reduction and analysis must be examined to highlight characteristics that influence the effectiveness of the design or capabilities of the operational air vehicle.

Methods for data reduction and analysis take many forms, but the objective is to present the data in a format most meaningful and useful to the end-user. In this case, the end-user is concerned with predicting the static and dynamic interaction between a radar and an air vehicle RCS. Three data processing techniques along with their advantages and disadvantages are summarized below.

2.4.1 Target Representation The first technique limits the amount of data by reducing the complexity of the target model. An experienced analyst identifies structures leading to large return such as engine cavities or concave dihedrals. The analyst simplifies the target model by representing the complex geometry with a simplified geometry composed of building blocks such as flat plates, cylinders, or conics. The analyst then calculates the RCS by direct calculation of Maxwell's equations or computer solutions, and sums the component RCS values. Blake (7) represents this approach with the formula

$$\sigma_{total} = |\sum_{k=1}^{N} \sqrt{\sigma_k} e^{\frac{i4\pi d_k}{\lambda}}|^2 \tag{5}$$

where N is the total number of scatterers, σ_k is the cross section of the kth scatterer, λ is the wavelength, and d_k is distance to the kth element from a reference plane perpendicular to the radar line of sight. This equation takes into account the relative phase angles of the separate scatterers.

The method is fairly simple and achieves adequate results for RCS estimation. However, the target representation relies on the experience of the analyst to accurately model the complex geometry using canonical scattering elements. This technique leads to a "first-look" RCS calculation and can vary widely from the exact solution. When combined with a motion model, the results could be inaccurate.

2.4.2 Full RCS Analysis A second approach is to make the maximum possible use of the predicted or measured raw data—no attempt is made to reduce the data set. The analyst combines the RCS data set with a motion model and calculates the detection based on the corresponding RCS value for each possible time instant.

This technique is useful because it can be used to determine aspect angles causing large values of RCS. But more importantly, it can be used to trace these values back to the sources in the geometry causing the large values of RCS. Additionally, this technique most accurately predicts the deterministic behavior between a radar and an air vehicle in a single-look engagement. However, when determining single-look detection, this technique is computationally burdensome and fails to model fluctuations induced by translational and rotational motions of the target, aeroelastic effects on the target, changes in the electromagnetic environment, unpredictability of the exact times at which the radar beam will sweep across the target, and errors in the prediction or measurement system.

2.4.3 Statistical Analysis The final approach models RCS as a continous random variable as discussed by Swerling (45) (46) and Welsh (55). This approach assumes that in a continuum of any range, an uncountably infinite number of possible RCS values exist. During any particular radar dwell, the target presents a set of aspect angles to the radar. Each RCS value corresponding to the aspect angle is in the subset of the full RCS and is within the neighborhood of a given range of angles. The radar selects an RCS value with equally random probability within this sector of RCS values. The basic priniciple then is to model the sector of data as a random variable by

14

calculating key statistical quantitiies such as mean, median, and variance. These values are then used to derive cumulative density function (CDF) and probability density functions (PDFs) of the RCS. The PDFs define theoretical models characterizing the RCS fluctuations and are used in calculating P_d. For air vechicles, the common models include the Swerling Case 1 (Rayleigh), Swerling Case 3, Weinstock, Beta, and log-normal.

Unlike deterministic methods, this approach is quite attractive for predicting single-look P_d. If sectorizing techniques are used as discussed in Chapter IV, the amount of data is significantly reduced with a corresponding reduction in time to calculate P_d. Swerling estimates the maximum number of sectors required to describe an air vehicle is less than 50. The problem arises in selecting the proper window size and accurately fitting the RCS distribution to a known PDF.

2.4.4 Summary The information provided in this chapter forms the basic framework for an intuitive understanding of volumetric RCS data. Serveral techniques are used to collect RCS data and each technique provides the designer or user with various degrees of RCS fidelity. As researchers improve the procedures used to calculate RCS, the techniques used to transform the data into meaningful information must also improve. The next chapter describes a potential solution to this problem by dicussing scientific visualization techniques for graphically displaying volumetric RCS data.

III. Scientific Visualization Techniques

3.1 Introduction

Recently, there has been an explosion in the amount of data generated by computers and computer-controlled measurement systems. The data originates from sources such as medical imaging systems, geographic mapping from satellites, computational chemistry programs, and others. The ability to generate computer images of this data is quickly becoming a potential solution for synthesizing vast quanitities of data and has led to a variety of methods used to view the data (52). Similarly, rendering techniques for displaying RCS data can draw from the experiences in scientific visualization of complex phenomena (12) (35) (34) (59) (32), medical imaging (41) (37) (50) (19), and scene generation (18) (38). In medical imaging, magnetic resonance imaging (MRI), computed tomography (CT) or single-photon emission computed tomography (SPECT) machines sample the body at fine degrees of detail and produce digitized, parallel 2D slices of volumetric data. In scientific visualization, computationally expensive equations like Navier-Stokes (computational fluid dynamics) produce vast quantities of scalar and vector data when calculating the air flow around a new aircraft wing design. In scene generation, producers demand more realism which increases the amount of detail in the scene, and typically, an increase in the data.

To draw on this experience and apply it to the problem of 3D visualization of volumetric RCS data, it is important to understand the various techniques and the capabilities and limitations of each one. This chapter presents a summary of the various computer graphics techniques available for 3D visualization of volumetric RCS data. The chapter focuses on three major rendering techniques available for display of this data: volume, surface, and particle systems rendering.

3.2 Volume Visualization Techniques

Kaufman (25) defines Volume Visualization as the process of directly generating a 2D image from a volumetric data set. The primary difference between volume rendering and surface render-

17

ing techniques is volume rendering directly renders the volumetric data without any intermediate conversion to a surface representation. The primitive element is a volume element or *voxel*, a parallel-piped shaped element of a 3D volume. The voxel is a small volume of data that has some numeric values representing a measurable attribute of the voxel. For example, in medical imaging, a voxel may represent the density values of the human tissue.

Yagel (57) states that one of the simplest ways to implement a volume renderer is to traverse the volume and transform each 3D point using the current transformation matrix and project the data into a Z-buffer . Each point in the Z-buffer is then drawn on the screen using the graphics hardware. One disadvantage of using this technique is the inability to render semi-transparent objects. To alleviate this problem, a back-to-front (BTF), also known as the painter's algorithm, or front-to-back (FTB) algorithm is used (19). In BTF, the voxel array is rendered in order of decreasing distance to the observer and in FTB, the voxels are rendered in increasing distance to the viewer. These compositing techniques allow for the passage of light and permit the rendering of translucent objects.

Another technique used for volume rendering is ray casting described by Levoy (29). A ray is cast from each pixel on the screen to the volume of data and accumulates opacity and color as it travels through the volume. The pixel is then displayed on the computer screen with the accumulated opacity and color. Ray casting only uses primary rays so it does not effectively simulate the interaction of light with an object. Ray tracing differs from ray casting by recursively following primary and secondary rays to accumulate color and opacity in the scene resulting in a more photo-realistic image.

A recently devolped technique for volume rendering is called splatting (56). Splatting is similar to FTB rendering, but the voxels are *splatted* onto the image plane. The center of the splat contains a high concentration of the pixel's contribution, but the contribution diminishes further away from the center.

18

Exceptional photorealism can be achieved with volume rendering techniques, but all techniques suffer from one disadvantage: all voxels contribute to the generation of the image and rendering time grows linearly with the size of the data set (29). Several techniques are used to speed-up volume rendering such as distributed networks used by Brightbill (8) and discrete ray tracing described by Yagel (58), but these techniques are still computationally intensive. Another disadvantage is that volume rendering algorithms are normally designed for uniform and non-uniform, regular rectilinear meshes and may require a preprocessing step to map the data values to a grid (22). See Tisdale for a discussion on the application of volume visualization rendering of RCS data (51).

3.3 Surface Rendering

Unlike volume visualization that directly renders the volumetric data, surface rendering techniques operate in two distinct stages. First, the data values of interest are extracted from the volumetric data and connected to form a surface The constructed surface is then rendered using standard surface rendering techniques.

3.3.1 Surface Construction

Several techniques exist for constructing a surface from a series of 2D parallel slices of volumetric data. The basic technique extracts and connects data points on one slice to points on its adjacent slice using polygons, bi-cubic, or quadric surface patches. If polygons are used, the result is usually a triangular mesh that forms a polyhedral approximation to the surface. Triangles are selected because of the speed associated with rendering this primitive polygon.

One surface construction technique extracts a surface of constant value from a volumetric data set. This algorithm, Lorensen and Cline's Marching Cubes (31), uses a divide and conquer approach to locate the surface in logical cubes created from eight grid points in the data set; four each from two adjacent slices of data. Scalar values at each vertex of the cube are compared against

a user-requested value to determine adjacent vertices which enclose the value. Linear interpolation is used to determine the location of the edge intersection. Each cube is then examined for its arrangement of edge intersections (up to 256), and triangles are used to connect the intersection points. The algorithm then marches to the next cube until it traverses the entire volumetric data set.

Another technique is based on the assumption that a data point on the contour of a surface is connected to a point on an adjacent contour. Extraction of the data points is not required because contours are represented by an ordered list of data points. Numerous algorithms have been implemented based on this technique such as Christiansen and Sederberg's algorithm (13) that connects a data point on one slice with the closest data point on the adjacent slice. For the most part, these algorithms work well if the contours are generally convex and mutually centered. If even one of these conditions is not satisfied, as shown in Figure 2a., the results may be incorrect as shown in Figure 2b. Several metrics may be applied to poorly-behaved data including "minimize area" used by Fuchs (21), or "maximize span length" as described by Christiansen (13). However, if the contours vary widely in shape, these algorithms can provide incaccurate result. Recently, Ekoule, et al. (16) described a general-purpose triangulation algorithm which automatically solves many of the problems associated with connecting adjacent contours of widely varying data. Ekoule's technique is applied in this work and is described in more detail in Chapter IV.

3.3.2 Rendering Once the surface is constructed, the object is rendered and displayed on the screen. During this phase, the visible surfaces are identified, lighting models are applied to determine surface colors, and the object is viewed interactively.

3.3.2.1 Visible Surface Identification The first step in generating the image is to identify the objects visible by the viewer. Objects outside the viewer's field of view are clipped, and objects inside the field of view are inspected to determine if the polygons are visible by the viewer.

20
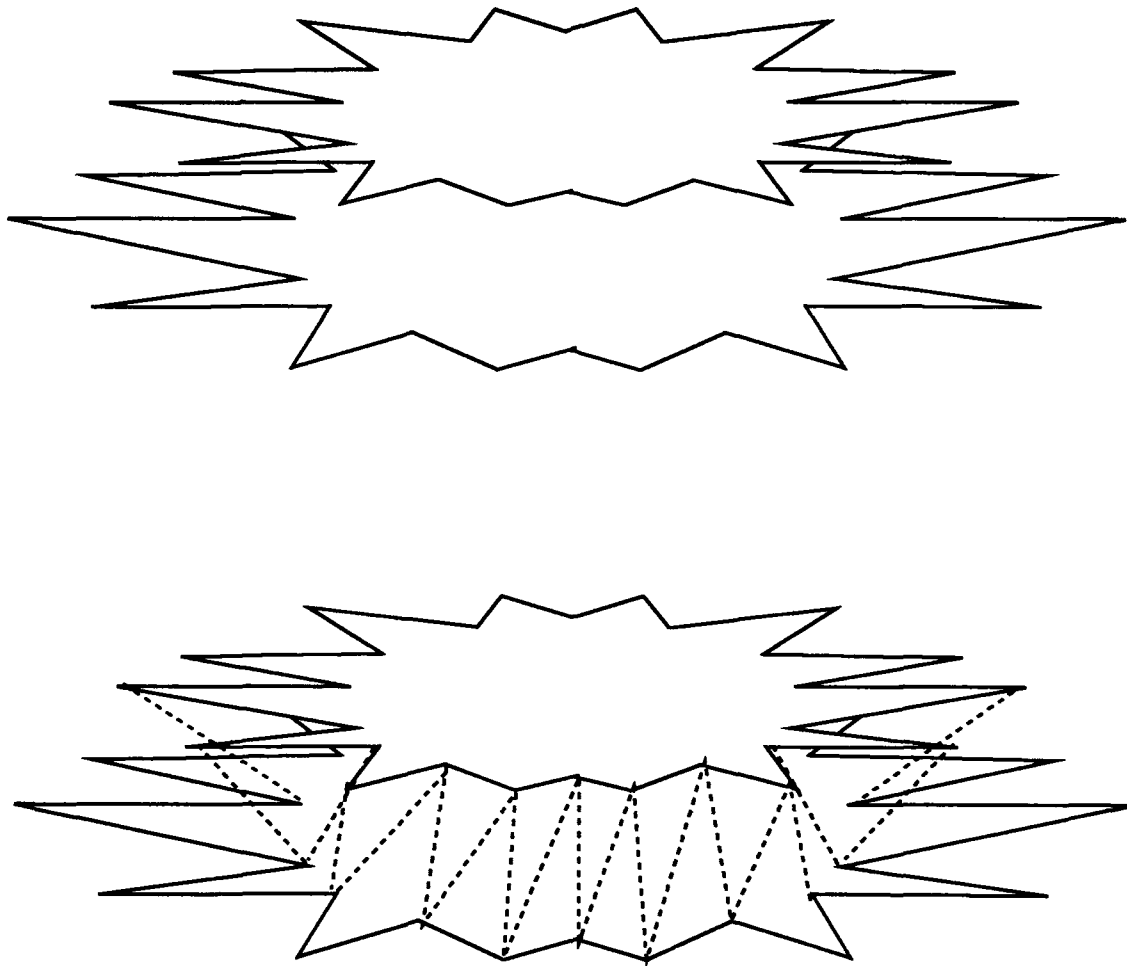
Figure 2.   a. Consecutive concave contours that pose a problem for conventional triangulation algorithms. b. Resulting triangulation using conventional triangulation algorithms

Several techniques are used to identify visible surfaces and remove hidden surfaces. Sutherland (42) groups these techniques into two main categories: image space and object space techniques. Image space techniques compare the surfaces of each object with a pixel to determine if the surface is visible. Object space techniques compare surfaces of each object to other surfaces in the scene to determine if the surface is visible.

The Z-buffer algorithm discussed earlier is an image space technique and is now standard on today's graphic's workstations. Carpenter's (11) A-buffer algorithm is similar to the Z-buffer algorithm. In addition to the x, y, z components of the surface, the A-buffer adds an alpha channel (α)

21

value to signify the opacity of the surface. For overlapping surfaces, the resulting image is determined by summing the opacity values of the component surfaces. This technique is used on today's graphics workstations and leads to improved photo-realism by easily implementing transparency.

Although most image space techniques operate on primitive surfaces, scan line conversion calculates the image pixel-by-pixel. The edge lines of the surfaces are sorted into *buckets* based on the edge's y-coordinate, and edges within the bucket sorted by the x-coordinate. The buckets are then processed from bottom to top and left to right across the scene (17).

Some object space algorithms sort the objects in the scene according to depth along the viewer's line of sight. The BTF and FTB algorithms previously discussed are examples of object space algorithms, but instead of rendering voxels, polygons are displayed in order of increasing or decreasing distance to the viewer.

3.3.2.2 Adding Color and Light Once the surface is constructed, lighting, shading, coloring, and other visual cues are added to the object to increase data comprehension. Dennis (15), Foley (17), and Kajiya (24) provide discussions on lighting and shading models and the use of spotlights, floodlights, etc. to increase realism. Robertson (39) and Ware (54) explain the use of effective coloring techniques using various color gamuts.

When we view an object in the real world, we see the intensity of the reflected light from the surface of the object. The light originates from various sources in the scene and we see the summation of those lights as they interact with the characteristics of the surfaces. In a simulated environment, the lights in the scene typically represent some real-world light source like the sun streaming through a window or a spotlight on a stage. In viewing scientific phenomena, however, there is no corrolary to real world light sources, so we are free to choose surface characteristics and lights that permit us to see the data most clearly.

Three surface characteristics contribute to the lighting models used in simulated environments. These empirical values are known as the ambient, specular, and diffuse coefficients. Am-

bient light is a non-directional source of light that equally strikes all objects in the scene. The ambient coefficient approximates the complex ways light indirectly reaches an object. The diffuse or *Lambertian* component describes the interaction between a light source and a viewer, that is the light intensity is proportional to the cosine of the angle between them. For example, if the diffuse component is 0.5 and the light source and viewer are separated by 45°, the viewer would see 35% of the original light source. The specular component describes the shininess of a surface and is based on the observation that light reflected from shiny surfaces can be approximated by $\cos^n \alpha$ where n is the specular reflection coefficient and α is the angle between the direction of reflection and the viewer. For a very shiny object like a mirror, $n \to \infty$ and the viewer only sees the light if aligned with the direction of specular reflection.

If we use the above light model to view a complex polyhedron, and we assume each surface is defined by a unique normal, the resulting surface looks faceted. Adding more polygons to approximate curved surfaces does not alleviate this problem because our eyes can still easily detect the intensity discontinuities caused by the Mach band effect along the polygon edges. It is well known that Gouraud shading diminishes the intensity discontinuities by interpolating the vertex intensities across the surface. This shading process requires the normal for each vertex, but if the vertex is not known, an effective technique is to average the normals of the surfaces sharing the vertex. With the diminished discontinuities, the objects appear much smoother with no increase in polygon count.

Color, like lighting and shading, adds to the realism of the objects in the scene, and in the case of scientific visualization, adds to better data comprehension. Several color systems exist such as Hue-Saturation-Value (HSV), and Commission Internationale de l'Éclairage (CIE), but most computer display devices use the Red-Green-Blue (RGB) color system. RGB is an additive color system used for illuminating pixels on the display device. In the RGB system, a user specifies a color by assigning values to each primary color. For example, cyan equates to an RGB triple of

(0.0, 1.0, 1.0). The values are then used to drive the voltage levels in the red, green, and blue electron guns in the computer monitor.

Color is used in many applications to reveal certain aspects of data. Many disciplines, like cartography, have standard colors to represent various qualities about the terrain. For univariate scienitific data, Ware (54) states that a common technique is to map the data values to the colors of the visible light spectrum—minimum values map to violet and maximums map to red.

3.3.2.3 Orienting the user Visualizing complex phenomena in 3D is a relatively new area of research. Often, the amount or type of data is too complex even for the human visual system. Kerlick (26) recommends one technique to enhance the interpretation of scientific data by introducing visual cues such as graphical icons, 3D cursors, particle tracers, and interactive "actors" to the scene. For example, an arrow can be used to represent the direction of a vector quantity, or a streamer can be used to trace vortices in a fluid. This approach contributes to overall data comprehension by providing the user with a well-known reference point.

3.4 Particle Systems

Unlike volume and surface generation techniques, which assume the user wishes to display the entire data set, particle systems may be used to model pieces of natural phenomena. The user defines inherent characteristics of the particle such as color, initial velocity, and lifetime. A particle system algorithm then uses these characteristics to generate thousands of particles to simulate the change of natural phenomena over time. Fournier, Fussell, and Carpenter (18) applied stochastic modeling techniques to create realistic images of terrain while Reeves and Blau (38) used probabilistic algorithms to create visually-detailed trees and grass in the forest scene from *The Adventures of Andre and Wally B*. Reeves and Blau used these techniques to model dynamic environments like fire in the *Genesis* scene from *Star Trek II*. Particle systems represent objects as clouds of primitive particles that occupy their volumes, rather than using more classical surface-

24

based representations such as polygons, patches, and quadric surfaces. The disadvantage of using particle systems rendering is that each renderer is normally application specific. See Tisdale (51) for a discussion on the application of particle systems rendering to volumetric RCS data.

The information provided in this chapter summarizes several computer graphics techniques that may be applicable to rendering volumetric RCS data. Each technique has inherent advantages and disadvantages, but to create an interactive RCS display environment, surface generation techniques are the only methods capable of achieving near-interactive display rates. The next chapter outlines the design and implementation of applying surface rendering techniques to the problem of visualizing volumetric RCS data

IV. RCS Visualization System Requirements, Design, and Implementation

4.1 Overview

The overall system requirement for this thesis is to develop a visualization system that allows a user to interactively view a volumetric RCS data set. An iterative, rapid-prototyping approach was used throughout this effort with emphasis placed on visualizing the results. This chapter presents the system requirements, design, and implementation issues that were factors in the development of a 3D RCS visualization system. The chapter is organized into five sections. The first section discusses general, system-level requirements. The second section details the method used to collect the RCS data and the impact of the data format on the design of the connection algorithm. The third section specifies the graphics-related implementation details of the RCS surface construction. The fourth section discusses data reduction methods that (1) improve the interactive speed of the display (2) can be used for visualizing statistical RCS data. The final section provides a chapter summary.

4.2 System Requirements and Constraints

4.2.1 Data Representation As discussed in Chapter III, several techniques exist for displaying volumetric data. Particle systems, voxels, polygonal models, and others have been used to represent a wide variety of objects. However, a polygonal model was chosen, specifically the triangle, because it is widely used in graphics applications and easiest to implement. Also, triangulating data points between successive slices of data is a well-known procedure for well-behaved data, and it was thought this procedure could be extended to RCS data. These factors, coupled with the selection of the hardware platform, drove the decision to represent the data as a triangular mesh.

4.2.2 Rendering Software Two rendering tools were available for this effort: The Satellite Modeler, a concurrent thesis effort by Pond (36), and The Advanced Visualizer, a commercial software product purchased through Wavefront Technologies (4). Both rendering products read a

26

specific file format containing a geometric description of the object. The user specifies a list of points followed by a topological description of the polyhedron. The user adds color, lighting, and texture information using keywords in the description file.

The Satellite Modeler provides the user with a basic set of tools for rendering and interactively viewing geometric objects. The user creates a geometric description using the Air Force Institute of Technology's Geometry format, and the Satellite Modeler renders the geometry. The user specifies starting locations for each object in the scene then interactively rotates, scales, or translates the objects. The source code for the Satellite Modeler provides the necessary hooks that allow the user to customize the user interface for a particular application.

The Advanced Visualizer (TAV) provides the user with a complete set of tools for creating geometric objects. The user adds color, transparency, and textures to the resulting objects, places them in a scene, then animates the geometry using a video composition tool. TAV is ideally suited for using the power of animation for presenting ideas, but does not permit the user the ability to easily change the perspective reference point in an interactive mode, nor does it allow the user to change the user interface.

Geometry descriptions were implemented for both the Satellite Modeler and The Advanced Visualizer early in the design phase, but the Satellite Modeler was selected because of its ability to interactively display 3D surfaces and the ease of extensibility to the user interface and image interaction software.

4.2.3 Coordinate System It is necessary to define a coordinate system to refer to positions of RCS data. The system normally used for radar analysis will be used; it is a modified spherical coordinate system with the target located at the origin. A point in this coordinate system is described with three values: ρ, θ and ϕ as shown in Figure 3. The coordinates represent the radial distance from the origin, and two orthogonal angle coordinates, respectively. The angular coordinates are sometimes called the elevation angle (θ) and the azimuth angle (ϕ) and together
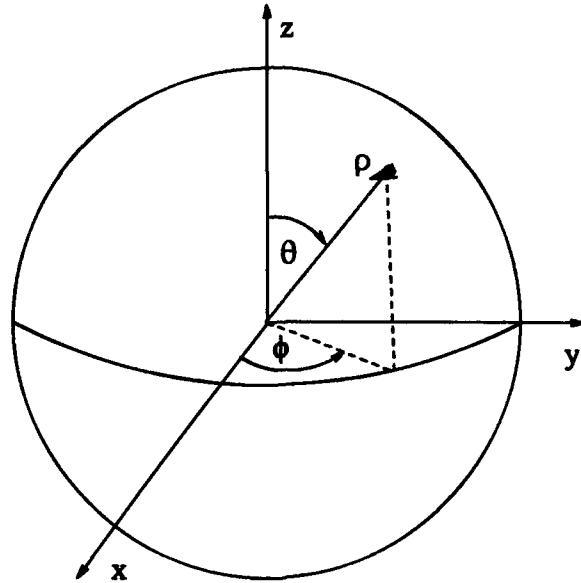
27

Figure 3. Radar analysis spherical coordinate system

comprise the *look angle*. In this coordinate system, ϕ will range from $0 - 360°$ whereas θ will range from 0 to $180°$.

4.2.4 Other Requirements A Silicon Graphics Iris-4D/440VGXT (2), with the associated Graphics Library was chosen for its optimized graphics pipeline. C++ was selected as the programming language because of its native ability to implement an object-oriented design. Additionally, C++ easily binds to the Silicon Graphics Graphics Library. The final requirement on the overall design was the amount of time alotted to implement the visualizer. This timing constraint necessitated a rapid-prototyping development and resulted in the most direct implementation of algorithms without much emphasis on code optimization. Emphasis was placed on the visualization of results.

4.3 Collection of 3D RCS Data

4.3.1 Requirements The main requirement for generating the image of 3D RCS data was to collect a sufficient amount of data on a representative, modern-day air vehicle. Additionally, the method of collection should be cost-effective and simple.

4.3.2 Design To create this dense data set, a computer prediction code was used because it is the most cost-effective technique to generate an unclassified, dense data set. Although many computer codes are available, Marhefka's (33) Radar Cross Section-Basic Scattering Code (RCS-BSC) is a user-oriented, cost-effective computer code that provides quick, representative results.

4.3.3 Implementation RCS-BSC accepts a geometrical description of the target as input. The input file contained a finite plate, perfectly conducting geometrical description of a modern conventional fighter aircraft as depicted in Figure 4. The user then supplies several input parameters. Because the overall objective of this thesis was to display a representative RCS, a compromise was made between input parameters leading to rigorous, mathematically correct results and characteristic results. The input parameters are presented along with a brief rationale for their selection.

1. Frequency = 1 GHz.

   For a complex target, it is well known that the rapidity at which RCS varies with respect to aspect angle is inversely proportional to the radar wavelength, i.e., a smaller wavelength produces a rapidly varying cross section. This frequency provided a compromise between slow (100 MHz) and highly rapid (10 GHz) variations in RCS and is a popular frequency for aircraft surveillance radars (40).

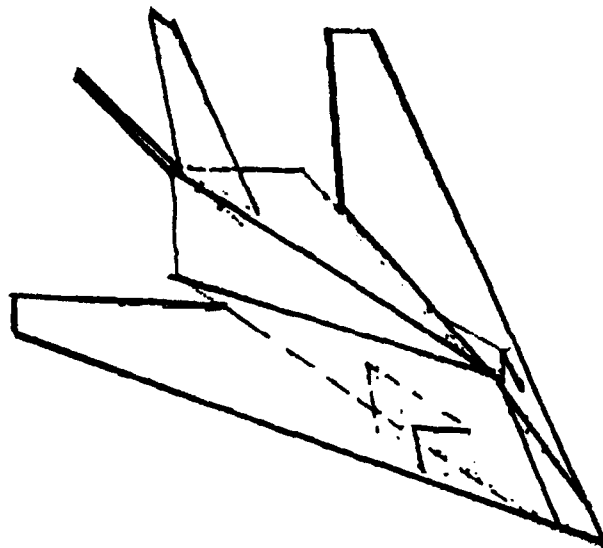2. Resolution in $\phi = 0.5° \sin \theta$

3. Resolution in $\theta = 0.5°$.

Figure 4. Modern conventional fighter used for input to RCS-BSC

Determining sampling requirements in ϕ and θ is an active area of research (48). A theoretical solution is based on the Nyquist sampling criterion, $\tan \theta = \frac{\lambda}{2L}$, where θ is the angular distance, λ is the wavelength, and L is the largest linear distance normal to the target line-of-sight (7). For a complex target, L is difficult to determine as the target rotates through an aspect angle. Therefore, a common estimation technique is to select L as some linear dimension roughly equal to the extent of the target (45). For this data set, $L = 20m$ resulting in an angular resolution of $0.5°$.

A constant sampling rate of $0.5°$ would have led to a non-uniform discretization as the sampling region approached the poles. To alleviate this problem, the angular resolution in ϕ was slightly modified to vary at $0.5° \sin \theta$.

The output of RCS-BSC is a series of RCS slices describing the right hemisphere of the volumetric data set. Each slice describes a contour of RCS for a fixed elevation angle and a varying azimuthal angle $(0 - 180°)$. A total of 84,000 data point descriptions were computed. Each point

30

at a particular aspect angle contains the magnitude in centibels (cB_{sm}) and phase information for $\sigma_{HH}, \sigma_{VV}, \sigma_{HV}$ and σ_{VH} as shown in Figure 5. The output of each slice was doubled to generate the left hemisphere of the data set, and was converted from centibels to decibels and into spherical coordinates. A sample of the converted data is shown in Figure 6.

```
679 185 -48   73 -41   85 680 184

497  66-748  86-290 217 504  65
544 267 152 274 150 272 545 269
485 114-608 233-168  58 478 114

382 149-890 217-305 117 372 153
390 356 145 330 143 340 392 356
459 218 131 107 135 115 465 221
469 309 148  53 139  60 463 311
346 169 126 177 120 192 343 170
403  38-605 166-158 338 409  38
```

Figure 5. Sample output format of RCS-BSC. The data sample contains magnitude (cB_{sm}) and phase information for $\sigma_{HH}, \sigma_{VV}, \sigma_{HV}$ and σ_{VH} for the top three contours of RCS data

```
  0   0  67.9 185 -4.8 73 -4.1   85  68.0  184

  0 0.5 49.7 66 -74.8 86 -29.0 217  50.4   65
 90 0.5 54.4 267  15.2 274  15.0 272  54.5  269
180 0.5 48.5 114 -60.8 233 -16.8  58  47.8  114
270 0.5 54.4 267  15.2 274  15.0 272  54.5  269

  0 1.0 38.2 49 -89.0 217 -30.5 117  37.2  153
 36 1.0 39.0 356  14.5 330  14.3 340  39.2  356
 72 1.0 45.9 218  13.1 107  13.5 115  46.5  221
108 1.0 46.9 309  14.8  53  13.9  60  46.3  311
144 1.0 34.6 169  12.6 177  12.0 192  34.3  170
180 1.0 40.3  38 -60.5 166 -15.8 338  40.9  38
216 1.0 34.6 169  12.6 177  12.0 192  34.3  170
252 1.0 46.9 309  14.8  53  13.9  60  46.3  311
288 1.0 45.9 218  13.1 107  13.5 115  46.5  221
324 1.0 39.0 356  14.5 330  14.3 340  39.2  356
```

Figure 6. Converted output format used for triangulation

4.4   Image Construction and Display

4.4.1   Requirements
As discussed in Chapter III, one of the approaches used in constructing a 3D surface of RCS data is to form triangular patches between consecutive slices of data. Once the image is constructed, visual cues are added to orient the user with respect to the data set.

4.4.2   Design and Implementation

4.4.2.1   Surface Construction
As shown in Figure 1, slices of RCS data are primarily concave and could pose a problem for conventional triangulation algorithms. Ekoule, et al. (16) proposed an algorithm that solves the problem of connecting concave contours. This technique preprocesses the data points along the contour by forming a *convex hull*. Thalman (49) states that a set of points is convex if a line segment joining any two pairs of its points is entirely contained within the set. Foley (17) provides a more intuitive definition by describing the convex hull as the polygon created by stretching a rubberband around the data points .

Figure 7a. shows the convex hulls of the object shown in Figure 2. Once the points are projected, the algorithm establishes a closest distance relation between a point on one contour and a point on an adjacent contour. The algorithm then steps around the contour pair and triangulates closest points as described by Christiansen (13). The result of this process is shown in Figure 7. This triangulation process is performed over successive pairs of contours and traverses the entire data set. Once the triangulation process is complete, a triangular mesh is formed by connecting the *original* data points.

4.4.2.2   Orientation Cues
In the traditional polar plot method of RCS data presentation, concentric circles are used to show relative magnitude with radial distance indicating strength of the RCS at a particular aspect angle. A similar technique was needed for 3D. It is well-known that color provides an additional visual cue for data comprehension, especially when applied to raised surfaces. While cartographers have a standard color scale to display height above sea-level,
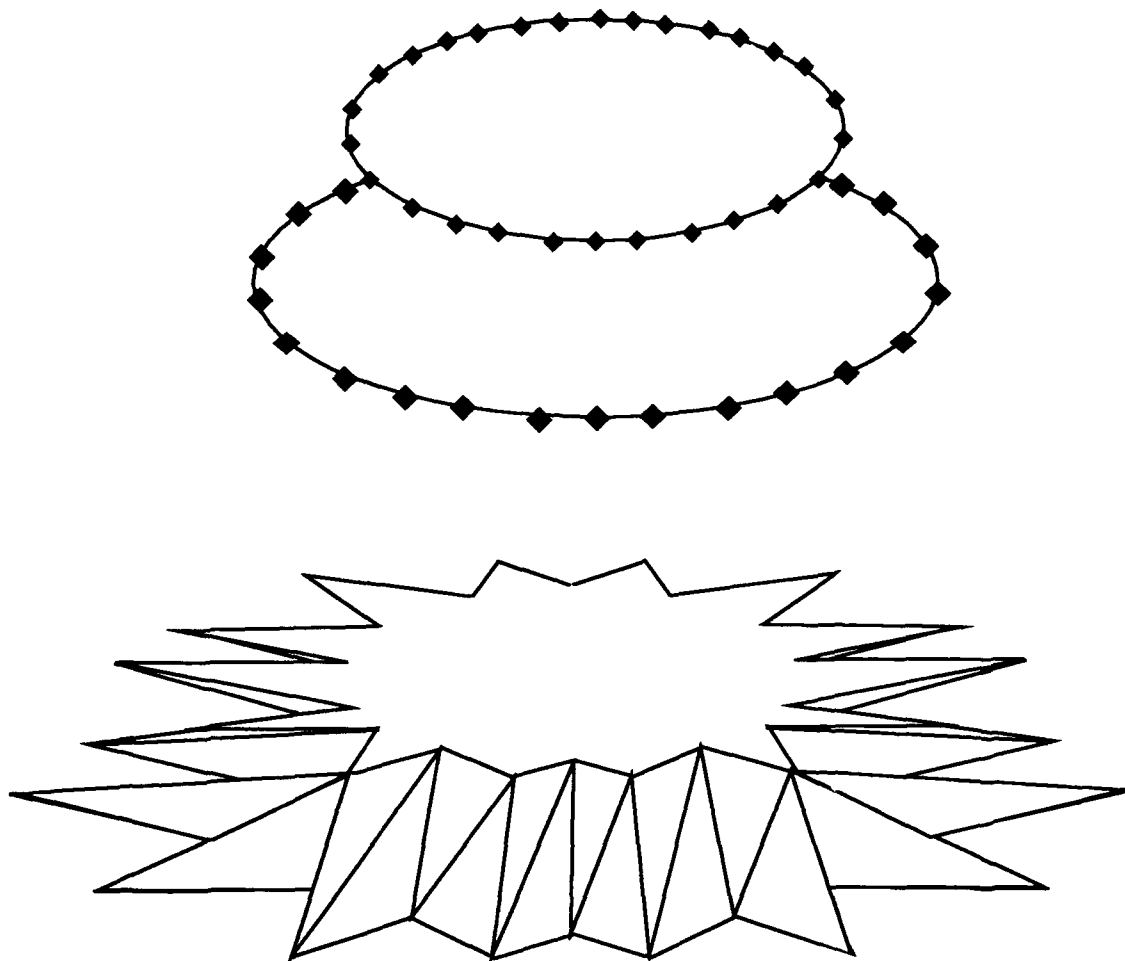
32

Figure 7.   a. Convex hull of Figure 2. b. Triangulation of adjacent contours using Ekoule's algorithm.

there is no standard for displaying RCS intensity levels. Conversely, the visible light spectrum is well-defined varying from violet ($400nm$) to red ($700nm$). Applying this principle to RCS intensity levels led to a monotonically varying color scale with violet indicating areas of weak scattering and red indicating areas of strong scattering.

Orienting the viewer with the RCS images proved to be a difficult design decision. Two approaches were implemented with varying results. Again, using traditional 2D polar plotting techniques, the air vehicle is positioned in the center of the plot as shown in Figure 1. Analogously, the air vehicle was placed in the center of the image and transparency was added to the RCS

surface. This technique worked well, but only when the RCS surface was limited to one color. When this technique was extended to interpolated colors, acceptable results could not be achieved. A potential reason for this problem is the sequence of calls needed to implement transparency. This sequence of calls may have occurred out of order and led to unsatisfactory results.

Transparency was shelved early in the design process, and instead, a separate window containing an icon of the air vehicle was used to provide the user with the necessary orientation cues. The icon simultaneously rotates with the RCS images.

The translation, rotation, zoom, lighting, and other tools provided by the Satellite Modeler were used to complete the visualization system.

4.5 Data Filtering

4.5.1 Requirements Two requirements were established for filtering the data set. Because rendering time is directly proportional to the number of polygons in the scene, the first requirement to reduce the raw data set to a level acceptable for *real-time* interactive display of the RCS images. For visual electromagnetics Cole (14) defines real-time as the time needed for the system to interactively respond to a change in the computational model with an upper bound of one minute. The second requirement was to describe the RCS image in such a way that the effective statistical characteristics of RCS are retained for use in a radar engagment.

4.5.2 Design

4.5.2.1 Simple Filter To meet the first requirement, a simple "local max" filter was developed. The user specifies a window size and the filter selects the largest value within the window. The non-overlapping filter then moves to the next window and repeats the process.

4.5.2.2 Statistical Filter The second data filtering technique is based on statistically characterizing the RCS of an air vehicle for input into a P_d model. Most of these data reduction

34

techniques are based on the work of Swerling and others as discussed in Chapter II. These techniques center on modeling the interaction between a dynamic air vehicle and a stationary radar as a statistical process.

Swerling (45) represents the target as a set of sectors (N_s) of potentially varying size. Each sector is described with the following characteristics:

- Four numbers specifying the sector boundary: Two for the midpoint and two for the sector widths

- One number specifying the mean (or median) within the sector

- At most two numbers specifying the RCS fluctuation law for the sector, i.e. Swerling Case 1, Log-normal, etc.

- One number specifying the correlation vs. angle increment for each sector.

To calculate sector size (Ω), Swerling defines two solid angles, Ω_1 and Ω_2, and recommends selecting the larger to define the overall sector (Ω). The following summary of this technique is presented without mathematical rigor and instead focuses on the intuitive understanding of determining sector size.

Ω_1 is the solid-angle region centered at an average look angle (ϕ, θ) and extending to a given sector width. The width is estimated based on the rotational and translational variations in the target's RCS from radar dwell to radar dwell.

Ω_2 is the solid-angle region in which target statistics are homogeneous, i.e. the medians and statistical fluctuation laws do not significantly change. Again, the solid angle is centered at an average look angle (ϕ, θ), but the extents vary according to the statistics of the target.

For example, suppose a radar is looking at an air vehicle at an average look angle of ($95°, -15°$) as shown in Figure 8. Because of the long time between successive radar dwells and the rotational/tranlational changes caused by air turbulence, the look angle changes by $\pm 2\frac{1}{2}°$. Ω_1, there-

fore, is centered at $(95°, -15°)$ with sector dimensions of $5° \times 5°$. Suppose Ω_2 of the same target is characterized by homogeneous statistics over the solid angle centered at $(95°, -15°)$ with sector dimensions of $40° \times 40°$. Since $\Omega_2 > \Omega_1$, the target statistics of Ω_2 would represent the RCS over the entire region centered at $(95°, -15°)$ and extending to sector width of $\pm 20°$.
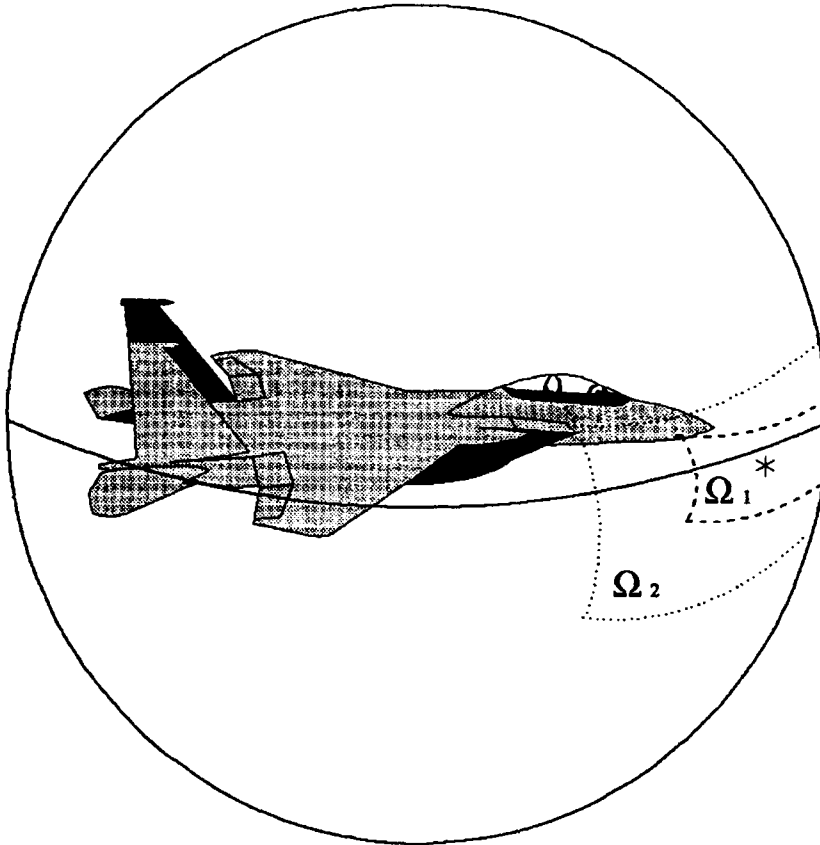

Figure 8. Sector definitions used for determining sector widths.

As stated earlier, this technique attempts to represent a continuous random variable by deriving an empirical distribution from a finite number of data points within a sector. This approach could lead to errors if enough samples are not used in the approximation. Therefore, another factor used in sectorizing the data is to ensure the number of data points within the sector (M) is large

36

enough to represent the RCS for a given confidence bound (β). For statistically representing RCS data, Swerling recommends $M = 101$ and $\beta = 0.05$.

4.5.3 Implementation The problem of statistically representing the RCS is reduced to identifying the size and statistical properties of the sector. Since the objective of the thesis was to visualize the statistical properties, the following implementation approach was used.

1. Assume the radar look angle changes slowly between successive radar dwells. This assumption leads to a small solid-angle region for Ω_1 and allows Ω_2 to be the driving factor in the determination of sector size.

2. Initially choose a solid-angle region of $\pm 2\frac{1}{2}^{\circ}$ to characterize Ω_2. This assumption best approximates a sector density (M) of 101 and a confidence factor (β) of 0.05. However, based on the data collection method used, the data near the polar regions becomes sparse. Therefore, this assumption is only valid between elevation angles of approximately $30 - 150^{\circ}$.

3. Assume the data within each sector to behave as a log-normal random variable. It is believed that log-normal models represent a class of targets similar to the model used for this thesis (47). Another reason for selecting a log-normal model to represent the sector statistics is that it allows determination about the behavior of the data within the sector. The mean-median ratio of the data within the sector is proportional to the variance. Large values in mean-median ratio (> 3) indicate log-normal statistics.

4. Apply coloring techniques and display the images side-by-side to identify two statistical characteristics of the fixed sector. On one image, the monotonically varying color scale represents the median value of the RCS within the sector. On the other image, contrasting colors identify sectors in which the data behaves log-normally.

This approach allows the user determine two properties of the RCS data set. First, the user can estimate the extents of Ω_2 by inspecting one image and combining adjacent sectors of similar

37

color. Second, the user can verify the statistical model used for a given sector by noting changes in the contrasting colors of the other image.

4.6   Summary

The requirements, design, and implementation issues discussed above provide the necessary information for building a RCS visualizer. The results of implementing the visualizer are discussed in the next chapter.

V. Results of the 3D RCS Visualization System

5.1 Introduction

The overall goal of this work was to design and implement an RCS visualization tool to be used by air vehicle designers, mission analysts, and pilots. The motivation for implementing such a tool was to exploit the capabilities of the human visual system by casting the data into an easier format to assist in the synthesis, design, and analysis of complex air vehicles. Since the output of the RCS visualization system is an image displayed on an interactive computer, it is impossible to adequately show its full capabilities. However, a sample of its output is presented in this chapter to show how the system can be used by various users. Several RCS analysts viewed the output of the visualization system to assist in the interpretation of the results. The first section is targeted to the air vehicle designer and electrical engineer by displaying the raw RCS data that may be used during design of an air vehicle. The second section targets the student of RCS by displaying the results of filtered data that sacrifice exactness for improved interactive viewing. The third section targets a pilot or mission analyst by displaying the potential interactions between an air vehicle and a potential threat radar. Each section includes a discussion of the rendering time and frame rates achieved with each image. The final section summarizes the results.

For each section, the following steps were used to generate the RCS image:

1. Filter the raw data, if applicable, using one of the techniques described in Chapter IV and produce a new data file.

2. Triangulate the data and produce a file to be read by the modified Satellite Modeler.

3. Display the data using the modified Satellite Modeler.

For each example, the visualization system transformed the data provided by RCS-BSC, and unless otherwise noted, displays only the σ_{VV} data set. Each image is shown from five separate perspective reference points with the image centered at the origin. The five perspectives are

39

- God's-eye View. Perspective reference point is along the positive z-axis.

- Devil's-eye View. Perspective reference point is along the negative z-axis.

- Nose-on View. Perspective reference point along the positive x-axis.

- Broad-side View. Perspective reference point along the positive y-axis.

- Tail-on View. Perspective reference point along the negative x-axis.

5.2 Raw Data

With increased emphasis on design and operation of Low Observable (LO) air vehicles, designers and engineers must balance a reduction in RCS with the aerodynamic requirements of the platform. Many different components contribute to the RCS of the air vehicle, and the designer must recognize not only the aspect angles creating large RCS, but more importantly, the contributing components creating the large RCS. The RCS visualization tool provides the former capability.

Figures 9, 10, 11, 12, and 13 show the five views of the raw RCS data set. The designer could display this image and immediately recognize aspect angles of large RCS returns. Notice the small, noisy RCS values at the nose and tail of the air vehicle and the large RCS values as the viewer approaches broad-side. Expect a large return at both poles because of the large specular aircraft component at the poles of the aircraft. Notice the small lobe at approximately $(0, 60)$ most likely caused by the shaping of the canopy.

Data Type	Polygon Count	Rendering Speed (sec)	Frame Rate
Raw	336,480	6000	46.5 sec/frame
Local Max (5° × 5°)	3364	5.5	1.8 frames/sec
Statistical (Two images) (5° x 5°)	6348	9.8	1.2 frames/sec

Table 1. Comparison of polygon count, rendering speed and frame rates for each type of data.

5.3 Simple Filtered Data

Most problems of interest to RCS researchers like aircraft designers and eleci.ical engineers require substantial amounts of time to derive an answer that even today's supercomputers cannot determine real-time solutions . The student of RCS, however, may only need to visualize a subset of the raw data set to increase understanding of the RCS (14).

Figures 14, 15, 16, 17, and 18 display the results of filtering the data set using the "local max" filter. This particular filter selected the largest value from a window of 5° × 5°. When compared to the previous figures, the surface retains the overall shape, but lacks the minute detail of the raw RCS. The overall polygon count is reduced from 336,480 to 3,364. This reduction in polygon count directly increases the rendering speed and frame rate of the image. As shown in table 1, the filtered data set is much more useful in an interactive display system because of the faster frame rates, but loses the exactness of the previous model.
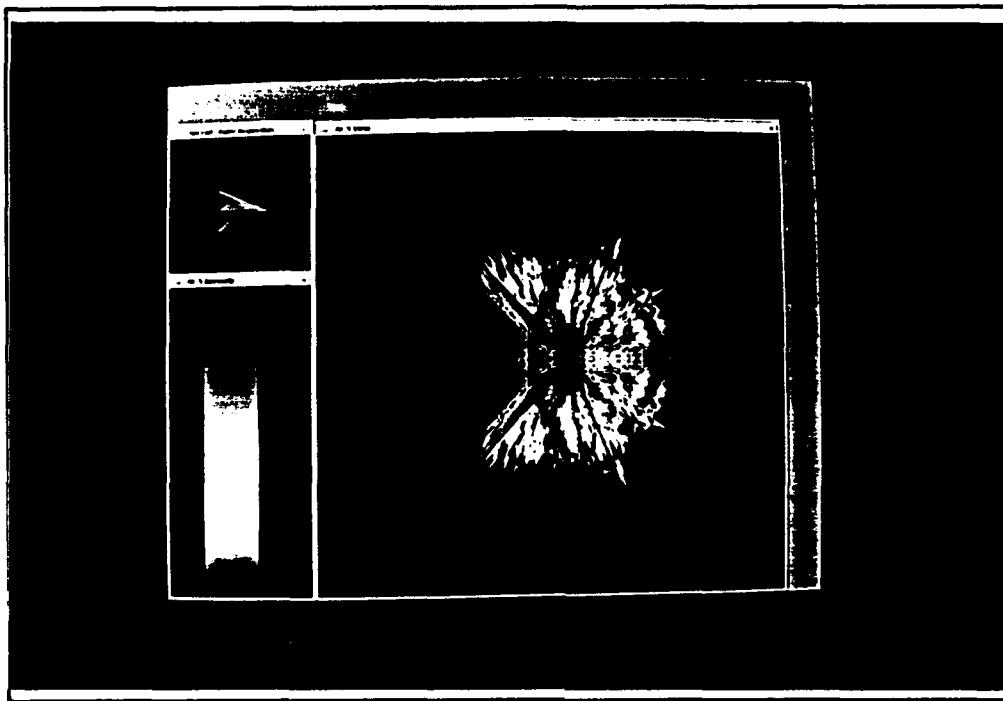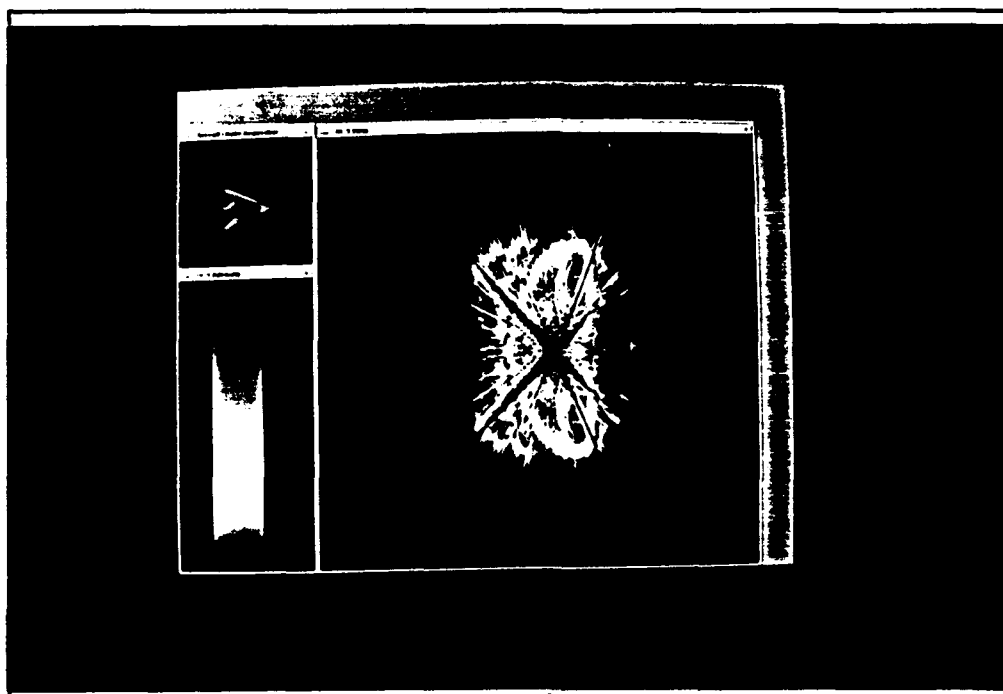
Figure 9. God's-eye view of raw data.

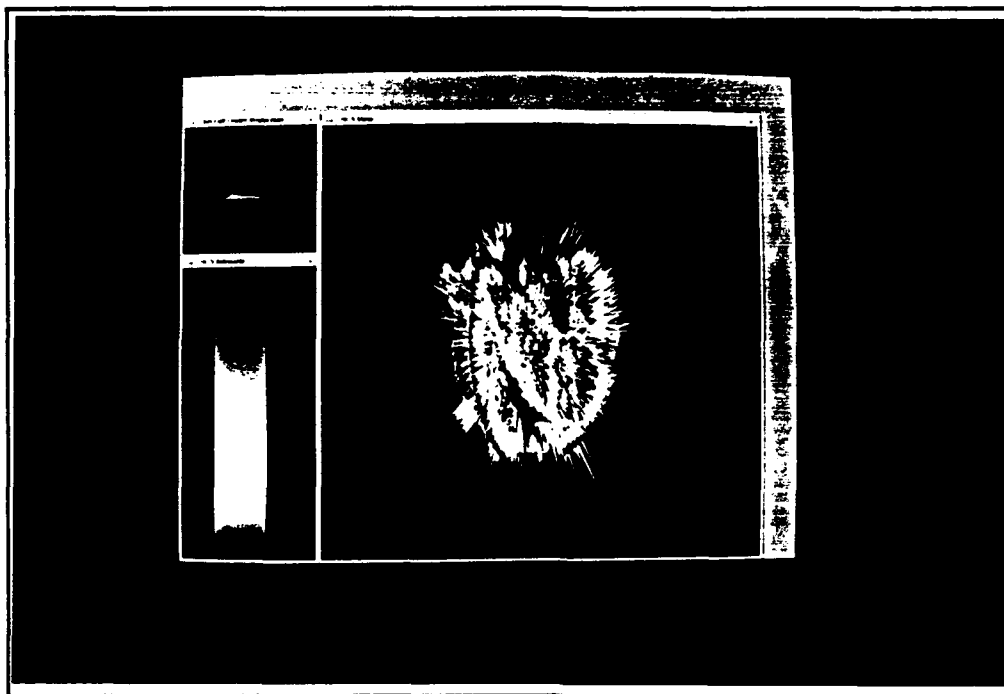Figure 10. Devil's-eye view of raw data.
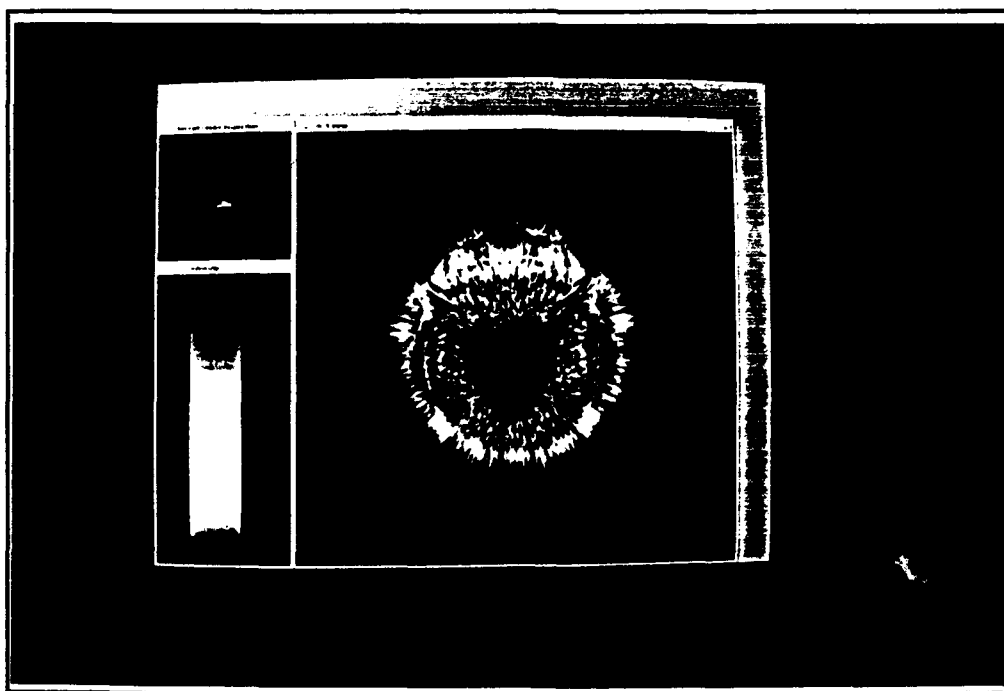
Figure 11. Broad-side view of raw data

Figure 12. Nose-on view of raw data set.

5.4 Statistically Filtered Data

To avoid detection and increase mission effectiveness, the mission analyst or pilot is concerned about the interactions between the air vehicle and a ground radar. Knowledge of this interaction allows pilots to completely avoid threats, or if that is not possible, steer the aircraft's RCS spikes through the radar's threat region. However, as discussed in Chapter IV, radar engagements are best characterized as a statistical function over a sector of data. Visualizing the statistical properties of the sector aids in the understanding of this interaction.

Figures 19, 20, 21, 22, and 23 display the results of filtering the data set using sector averaging techniques with a fixed sector of 5° × 5°. The image on the right uses color and shape to show the median RCS within a sector, and the image on the left uses color to compare the variance of the data within each sector. In this example, the red sectors have a variance greater than three and indicate sectors that accurately model log-normal data.

The pilot can examine the images and determine sectors of data that may lead to a decrease in P_d. For example, the sector surrounding the nose of the vehicle (Figure 22) indicates the aircraft displays both low observability and homogeneous statistics. A mission analyst may use the images to determine if a particular statistical model accurately describes the data within a sector. In this example, the analyst may model all red sectors as log-normal PDFs, but use a different model for the blue sectors.

The other benefit of depicting the data in this format is the overall speedup in the display of the data. Table 1 shows this filtering technique reduces overall polygon count to 6,378 and allows the display to reach near-interactive speeds.
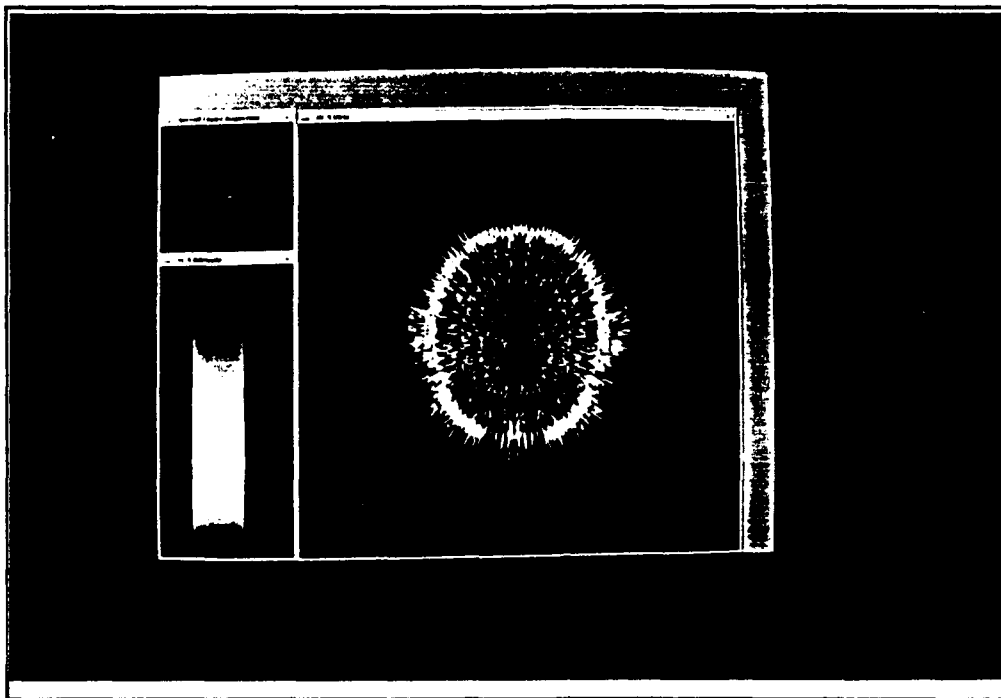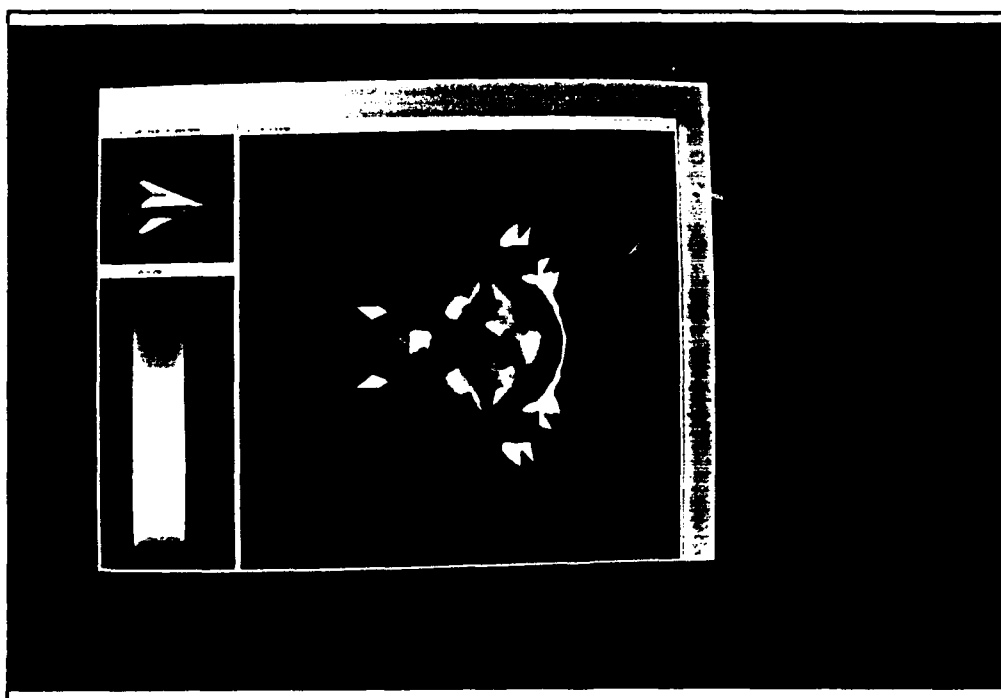
44

Figure 13. Tail-on view of raw data set.

Figure 14. God's-eye view of data filtered over a 5° x 5° window.

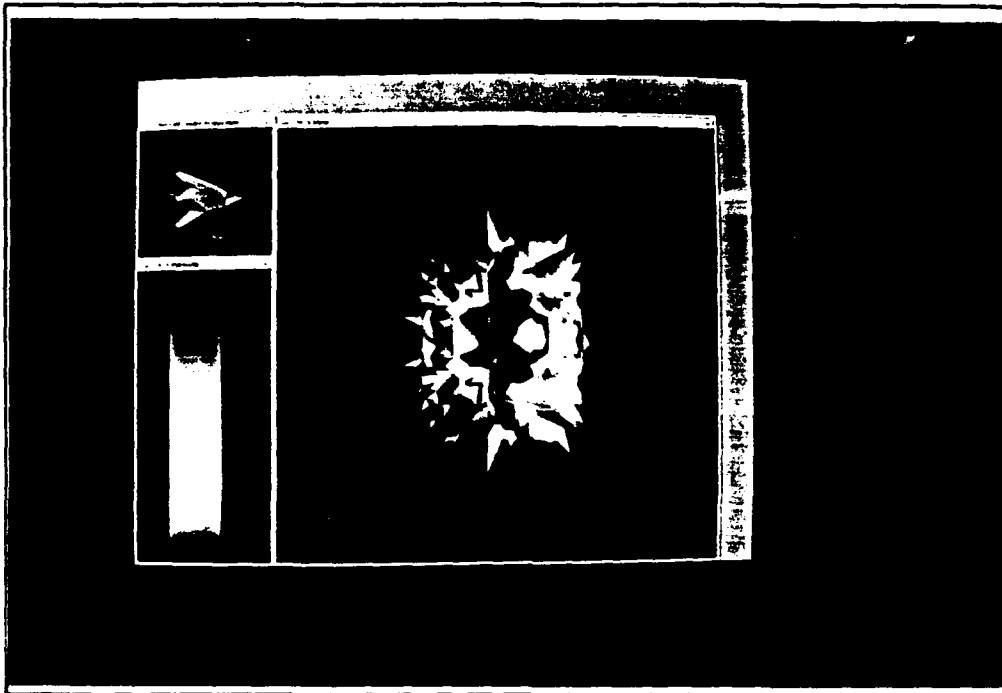Figure 15. Devil's-eye view of data filtered over a 5° × 5° window.

Figure 16. Broad-side view of data filtered over a 5° × 5° window.
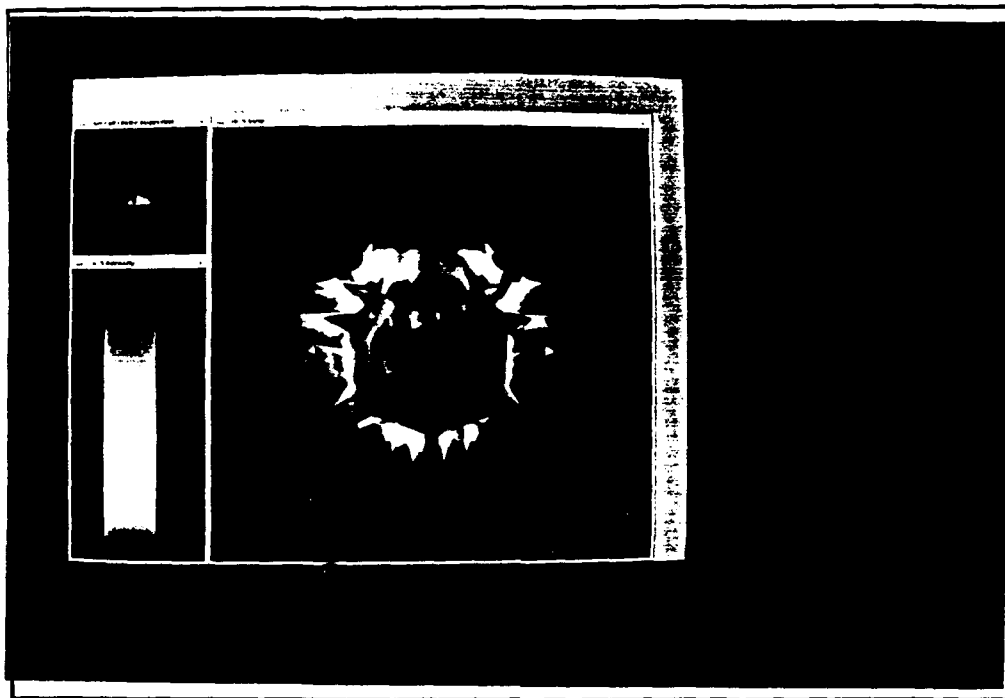
Figure 17. Nose-on view of data filtered over a 5° × 5° window.
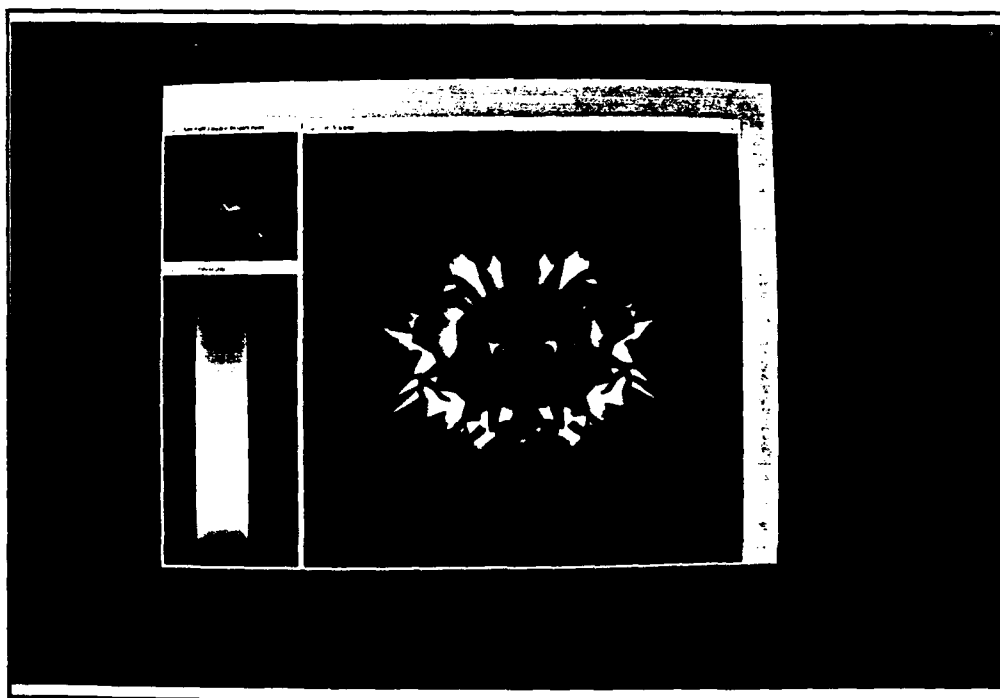
Figure 18. Tail-on view of data filtered over a 5° × 5° window.
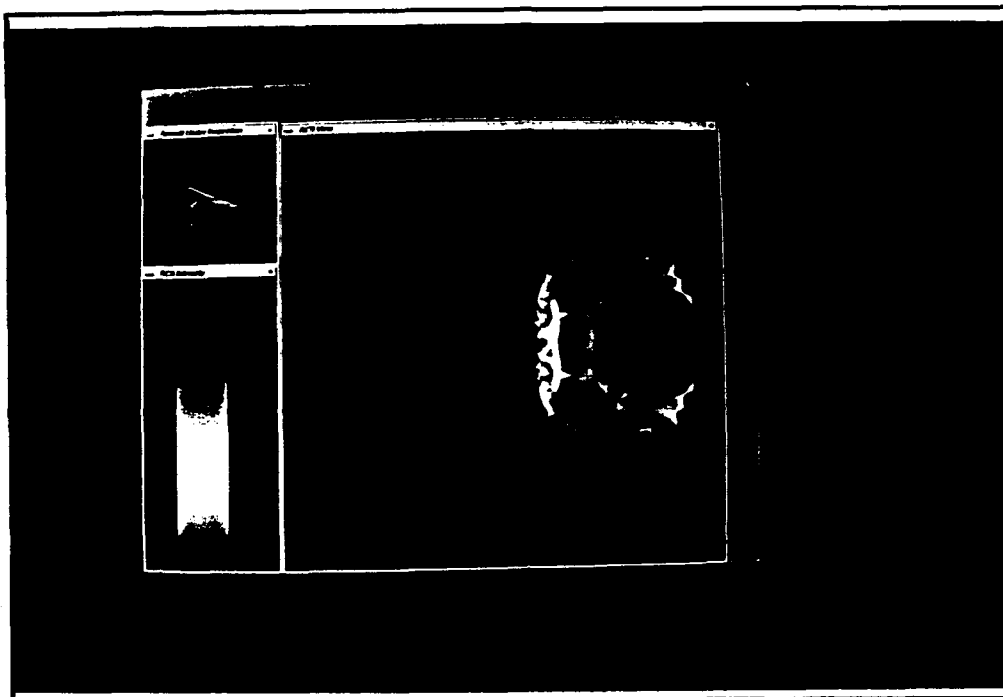
Figure 19. God's-eye view of statistical RCS data over a 5° × 5° window

5.5 Summary

In this chapter, three types of RCS data have been presented along with the interpretation of the images resulting from visulizing the volumetric data sets. The results have varying applications to the many individuals involved in the design, analysis, and operation of LO air vehicles.

Figure 20. Devil's-eye view of statistical RCS data over a 5° × 5° window

Figure 21. Broad-side view of statistical RCS data over a 5° × 5° window

Figure 22. Nose-on view of statistical RCS data over a 5° × 5° window.

Figure 23. Tail-on view of statistical RCS data over a 5° × 5° window.

VI. Conclusions and Recommendations for Future Work
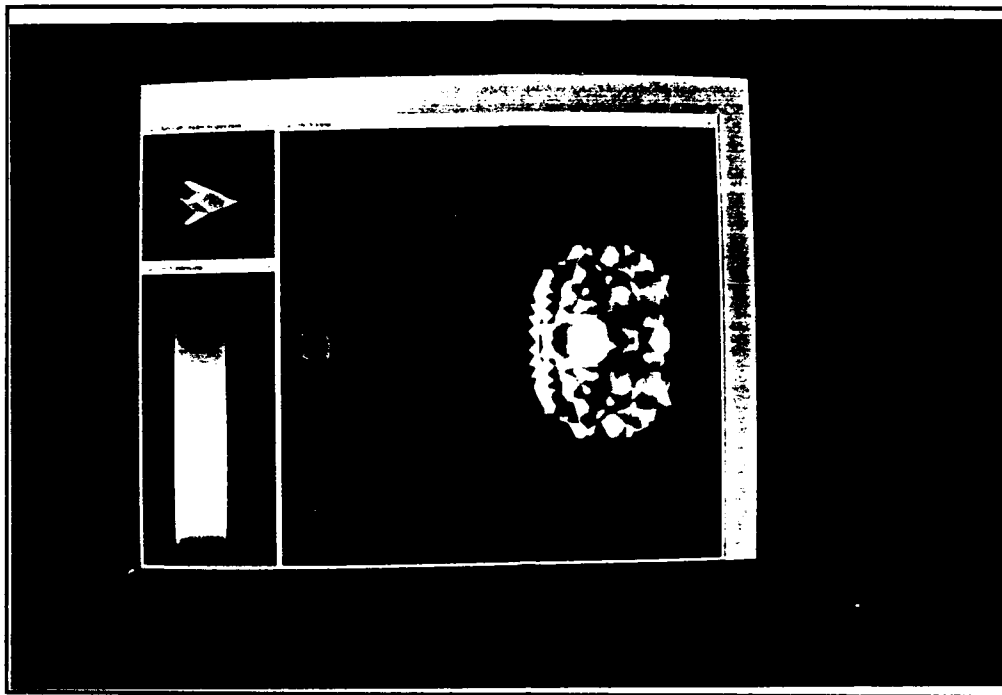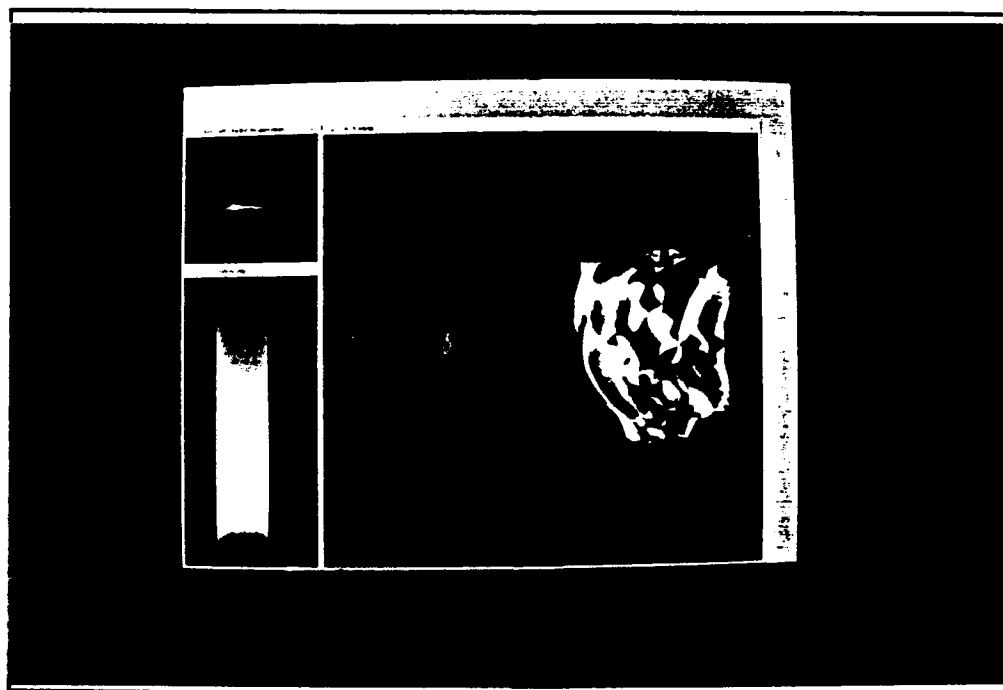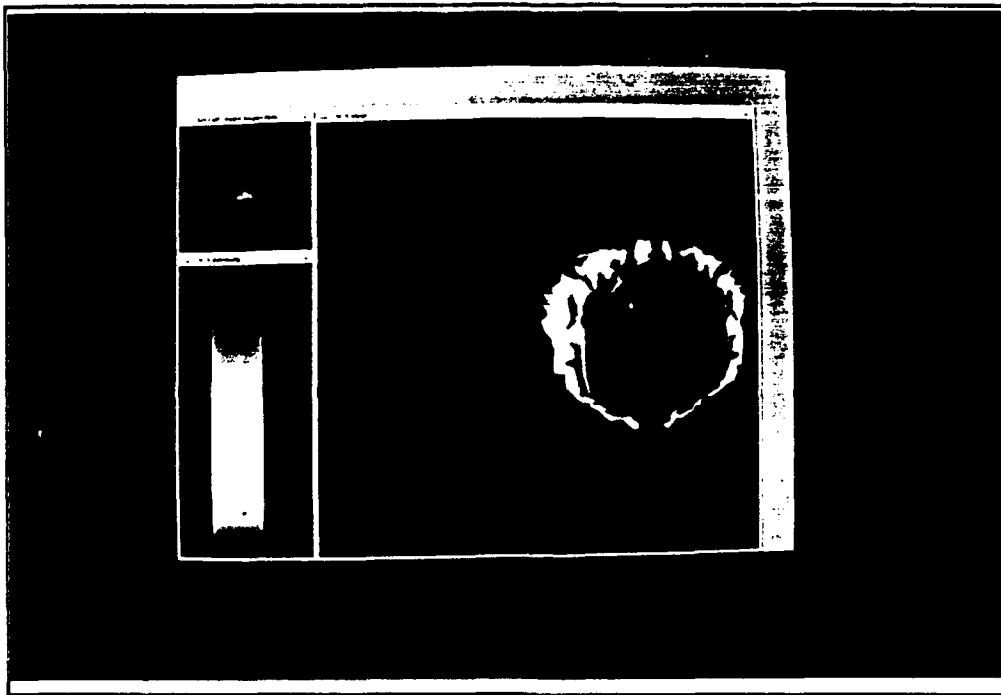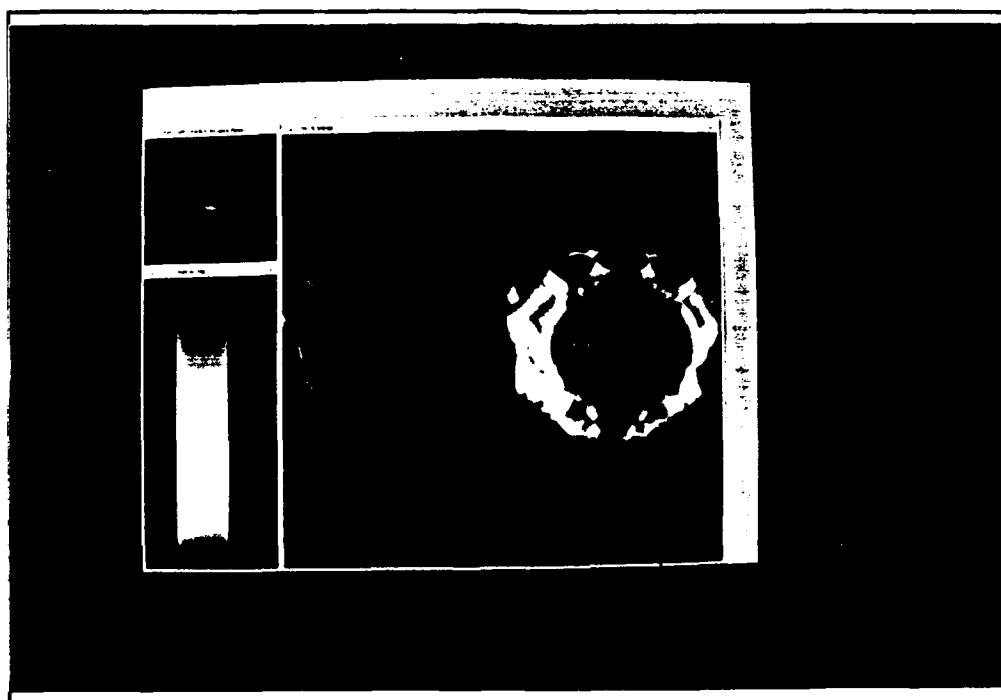
6.1 Introduction

The goal of this thesis was to exploit the human visual system to better understand the concept of RCS and the interaction of RCS with threat radars. To achieve this goal, an interactive, 3D RCS visualization tool was developed for use by engineers, air vehicle designers, mission analysts, and pilots. This chapter presents my concluding remarks about this work and recommendations for future work.

6.2 Conclusions

Visualization, through rendering of volumetric data, provides a valuable tool for extracting meaning from predicted or measured RCS data. By forming a volumetric surface from a set of 2D polar plots, adding variable color and orientation icons, and using the capabilities of a graphics workstation, the user is capable of identifying look angles that potentially specify areas of large RCS. The tool is capable of rendering a full 4π steradian data set sampled at fine intervals, or a statistical representation of an air vehicle as it may appear in an engagement with a ground radar. This leads to a better synthesis of RCS and analysis of the air vehicle design or planned mission route.

The results of this research have wide and varying applications. The first application is to give the RCS student a tool to better understand the concept of radar cross section. Too often, RCS is looked upon as a single value representing some nebulous quality about an air vehicle. This tool easily shows that RCS is a multi-valued quantity dependent on look angle, frequency, and polarization. It is important, especially in the age of low observable air vehicle design, that all individuals associated with a LO air vehicle understand its value and its limitations.

Another application is to give a powerful tool to air vehicle designers and electrical engineers. Historically, RCS data has been collected at a single elevation angle, and many extrapolations have

been based on this elevation angle. This tool allows the designers and engineers to see how quickly RCS varies in elevation as well as azimuth.

Finally, but most importantly, this tool gives the power of visualization to the operator of the air vehicle. Previously, the mission analyst or pilot used crude paper models or computationally expensive tools to determine an effective mission profile. This tool, coupled with a threat and terrain model, potentially allows the analyst or pilot to visualize the interactions between his air vehicle and a ground radar to select the most effective mission route to and from the target area.

6.3 Recommendations for Future Work

The RCS visualization tool developed for this work met its objectives, but it is by no means a complete tool and has only scratched the surface of RCS visualization. If anything, the tool has heightened the awareness of 3D RCS calculation and visualization and most of my recommendations are based on this observation.

6.3.1 Recommendations for Improved Visualization Research in the visualization of radar cross section must continue. Advances in the power of engineering workstations has moved the prediction of RCS from the supercomputer to the engineer's desktop. As electrical engineers continue to refine the process of calculating RCS, larger amounts of data must be sorted and analyzed. At the same time recent advances in computer graphics workstations allow for the rapid processing and visualization of more and more data.

The RCS visualization system should be incorporated into an overall air vehicle design tool. The RCS visualization system described in this thesis only visualizes volumetric RCS data—it does not trace the RCS back to the scattering centers responsible for creating the large values of RCS. Ideally, an interactive tool that combines CAD, RCS calculation, RCS visualization, and scattering center visualization, each simultaneously operating in a separate window, provides an air vehicle designer with the capability to visualize the balance between aerodynamic requirements and LO

requirements. Additionally, it would allow the student of RCS reduction techniques to experiment between the various design trade-offs and immediately see the effects of the changes.

Another approach is to place the air vehicle and the corresponding RCS image into a synthetic environment. This approach would allow the designer to interactively change the air vehicle's shape or construction and see the corresponding change in the RCS. Bryson and Levitt (10) describe a virtual windtunnel to explore the air flow around an air vehicle and a similar approach could be applied to visualizing volumetric RCS data.

Similarly, placing the air vehicle and its corresponding RCS image into a synthetic tactical battlefield would provide pilots and air-land battle planners the capability to visualize the value of reduced RCS. The synthetic battlefield could be used in the validation step of a proposed air vehicle or allow pilots to rehearse new weapons and tactics by witnessing the interactions between their actions and a threat radar.

The previous recommendations may require extensive time and effort, but a relatively simple speed-up technique for display of RCS data is to define the RCS mesh as an ordered list of triangles and take advantage of the t-mesh generator on the Silicon Graphics workstation. This approach should improve the frame rate for a dense data set by achieving the advertised rendering speed of the Silicon Graphics Iris 4D/440VGXT (1 million Gouraud-shaded polygons per second).

6.3.2 RCS Data Filtering Techniques Although reduction of RCS data was not the main objective of this thesis, I believe this research has opened the door for further discussion in this area. The question of reducing RCS data to a more manageable data set is dependent on the application of the data and is an ongoing area of research.

For the application of single-look detection, Swerling proposes sectorizing the data into a much smaller characterization, perhaps 50 sectors. Much of his published work, however, is limited to small data sets with limited elevation data. Now that 4π steradian data sets are readily available, his theoretical techniques should be extended to and verified for 3D.

53

Finally, research in data reduction techniques and statistical processing of RCS must continue. Perhaps someone will answer the question I encountered most often in my research—what data do you *really* need to effectively characterize a radar cross section?

Bibliography

1. *Radar Target Scatter (RATSCAT) Facility Capabilities Brochure*. Holloman Air Force Base, NM, 1986.

2. *Iris-4D Series Owner's Guide (Version 4.0)*. Mountanin View, CA, 1989.

3. *Tactical Air Command/Special Operations Forces (TAC/SOF) Requirements Document for the Automatic Mission Planner (AMP) Technology Development*. Warminster, PA, 1990.

4. *The Advanced Visualizer(Version 2.0) User's Manual*. Santa Barbara, CA, 1992.

5. Andersh, Captain Dennis, "Briefing Presented at Radar Signature Synthesis Program Review." Wright-Patterson AFB, OH, July 1992.

6. Balanis, Constantine A. *Antenna Theory Analysis and Design*. New York: Harper-Row, 1982.

7. Blake, Lamont V. *Radar Range-Performance Analysis*. Dedham, MA: Artech, 1986.

8. Brightbill, Captain Patricia. *Distributed Ray Casting for High-Speed Volume Rendering*. MS thesis, Air Force Institute of Technology, January 1992.

9. Brown, Alan, "Course Handout distributed in WENE 445, Short Course on Low Observables." Air Force Institute of Technology, Wright-Patterson AFB, OH, September 1992.

10. Bryson, Steve and Creon Levitt. "The Virtual Windtunnel: An Environment for the Exploration of Three-Deimensional Unsteady Flows," *IEEE Computer Graphics and Applications*, 17–24 (March 1991).

11. Carpenter, L. "The A-buffer, an Anti-aliased Hidden Surface Method," *Proceedings of SIGGRAPH 84*, 103–108 (July 1984).

12. Chakrabati, S., et al. "Visualizing Radiation Patterns of Antennas," *IEEE Computer Graphics and Applications*, 41–49 (January 1990).

13. Christiansen, H.N. and T.W. Sederberg. "Conversion of Complex Contour Line Definition Into Polygonal Element Mosaic," *Computer Graphics*, *12*(3):187–192 (July 1978).

14. Cole, Rodney W., et al. "Learning About Fields and Waves Using Visual Electromagnetics," *IEEE Transactions on Education*, *33*(1):81–94 (February 1990).

15. Dennis, Alan R. "An Overview of Rendering Techniques," *Computers and Graphics*, *14*(1):101–115 (1990).

16. Ekoule, A., et al. "A Triangulation Algorithm from Arbitrary Shaped Multiple Planar Contours," *ACM Transactions on Graphics*, 182–199 (April 1991).

17. Foley, James D., et al. *Computer Graphics Principles and Practice*. Reading, Massachusetts: Addison-Wesley, 1990.

18. Fournier, A., et al. "Computer Rendering of Stochastic Models," *Communications of the ACM*, *25*(6):371–384 (June 1982).

19. Frieder, Gideon, et al. "Back-to-Front Display of Voxel-Based Objects," *IEEE Computer Graphics and Applications*, *5*(1):52–60 (January 1985).

20. Fruhauf, M. "Volume Visualization on Workstations: Image Quality and Efficiency of Different Techniques," *Computers and Graphics*, *15*(1):101–107 (1991).

21. Fuchs, H., et al. "Optical Surface Reconstruction From Planar Contours," *Communications of the ACM*, *20*(10):693–702 (October 1977).

22. Giertsen, A. "Volume Visualization of Sparse Irregular Meshes," *IEEE Computer Graphcis and Applications*, 40–48 (May 1992).

23. Jackson, J., "The Data Transport Computer: A 3-Dimensional Massively Parallel SIMD Computer," 1991. submitted for publication.

24. Kajiya, James T. "The Rendering Equation," *Proceedings of SIGGRAPH 86*, *20*(4):143–150 (August 1986).

25. Kaufman, Arie, "Introduction to Volume Visualization, Course Notes for Introduction to Volume Visualization." ACM SIGGRAPH 92, Chicago, IL, July 1992.

26. Kerlick, G. David, "Moving Iconic Objects in Scientific Visualization, Course notes for Introduction to Scientific Visualization Tool and Techniques." ACM SIGGRAPH 92, Chicago, IL, July 1992.

27. Knott, Eugene F., et al. *Radar Cross Section Its Prediction, Measurement and Reduction.* Dedham, MA: Artech, 1985.

28. Lees, P. and M. Davies. "Computer Predictions of RCS for Military Targets," *IEE Proceedings*, *137*(4):229–236 (August 1990).

29. Levoy, M. "Efficient Ray Tracing of Volume Data," *ACM Transactions on Graphics*, *9*(3):245–261 (July 1990).

30. Loh, Gen J.M. "Advocating Mission Need in Tomorrow's World," *Airpower Journal*, *6*(1):4–13 (Spring 1992).

31. Lorensen, W. and H. Cline. "Marching Cubes A high Resolution 3-D Surface Construction Algorithm," *Proceedings of SIGGRAPH 87*, *21*(4):163–169 (July 1987).

32. Lorensen, W. and Boris Yamrom. "Golf Green Visualization," *IEEE Computer Graphics and Applications*, *12*(4):35–44 (July 1992).

33. Marhefka, R. J. *Radar Cross Section - Basic Scattering Code, RCS-BSC (Version 2.0) User's Manual.* The Ohio State University, Department of Electrical Engineering, Columbus, OH 43212, 1990.

34. Neal, M. "When Did Scientific Visualization Really Begin," *IEEE Computer Graphics and Applications*, 8–9 (November 1988).

35. Nielson, G. "Visualization in Scientific and Engineering Computation," *Computer*, *24*(9):58–66 (September 1991).

36. Pond., Captain David. *A Synthetic Environment for Satellite Modeling and Satellite Orbital Analysis.* MS thesis, Air Force Institute of Technology, December 1992.

37. Raya, S. and J. Udupa. "Shape-Based Interpolation of Multi-dimensional Objects," *IEEE Transactions on Medical Imaging*, *9*(1):32–42 (March 1990).

38. Reeves, W. and R. Blau. "Approximate and Probabilistic Algorithms for Shading and Rendering Structured Particle Systems," *Proceedings of SIGGRAPH '85*, *19*(3):313–322 (July 1985).

39. Robertson, P. K. "Visualizing Color Gamuts: A User Interface for the Effective Use of Perceptual Color Spaces in Data Displays," *IEEE Computer Graphics and Applications*, 50–64 (September 1988).

40. Skolnik, M. *Radar Handbook.* New York: McGraw-Hill, 1970.

41. Stytz, M. and O. Frieder. "Computer Systems for Three-Dimensional Diagnostic Imaging: An Examination of the State of the Art," *Critical Reviews in Biomedical Engineering*, *19*:1–45 (1991).

42. Sutherland, J., et al. "A Characterization of Ten Hidden Surface algorithms," *Computer Surveys*, *1*(6):1–55 (1974).

43. Sweetman, Bill. *Stealth Aircraft, Secrets of Future Airpower*. Osceola, WI: Motorbooks International, 1986.

44. Swerling, P. "Recent Developments in Target Models for Radar Detection Analysis," *Proceedings of the AGARD Avionics Technical Symposium on Advanced Radar Systems* (May 1970).

45. Swerling, P. "Radar Target and Signal Fluctuation Models." , September 1992.

46. Swerling, P. "Sectorized Statistical Target RCS Characterizations." , September 1992.

47. Swerling, Peter, President of Swerling Mannasse and Smith. Personal interview. Woodland Hills, CA, October 1992.

48. Terzuoli, Andrew Jr., "Course Handout distributed in WENE 445, Short Course on Low Observables." Air Force Institute of Technology, Wright-Patterson AFB, OH, September 1992.

49. Thalman, Daniel. *Scientific Visualization and Graphics Simulation*. Chichester: John Wiley and Sons, 1990.

50. Tiede, U., et al. "Investigations of Medical 3-D Rendering Algorithms," *IEEE Computer Graphics and Applications*, 41–53 (March 1990).

51. Tisdale, Captain David. *Methods for Viewing RCS Data in 3D*. MS thesis, Air Force Institute of Technology, December 1992.

52. Treinish, Lloyd A., "Introduction to Data Management Methods for Scientific Visualization, Course Notes for Introduction to Scientific Visualization." ACM SIGGRAPH 92, Chicago, IL, July 1992.

53. Turner, S. "RESPECT: Rapid Electromagnetic Scattering Predictor for Extremely Complex Targets," *IEE Proceedings*, *137*(4):214–220 (August 1990).

54. Ware, C. "Color Sequences for Univariate Maps: Theory, Experiments, and Principles," *IEEE Computer Graphics and Applications*, 41–49 (September 1988).

55. Welsh, Byron. "Statistical Processing of Radar Cross Section Data," *Proceedings of the 30th Annual Joint Electronic Warfare Conference* (9 1985).

56. Westover, L. "Footprint Evaluation for Volume Rendering," *Computer Graphics*, *24*(4):367–376 (August 1990).

57. Yagel, Roni, "Methods for Volume Viewing, Course Notes for Introduction to Volume Visualization." ACM SIGGRAPH 92, Chicago, IL, July 1992.

58. Yagel, Roni, et al. "Discrete Ray Tracing," *IEEE Computer Graphics and ApplicaitionsComputers and Graphics*, *12*(1):19–28 (September 1992).

59. Yasuda, Takami, et al. "3D Visualization of an Ancient Egyptian Mummy," *IEEE Computer Grpahics and Applications*, *12*(3):13–17 (May 1992).

Vita

Captain Thomas G. Wojszynski was born on 18 October 1960 in Pittsburgh, PA and graduated from Bethel Park Senior High School, Bethel Park, PA in 1978. Tom enlisted in the U.S. Air Force in 1978, and following basic military training attended Russian language training at the Defense Language Institute in Monterey, CA and Goodfellow AFB, TX. Upon completion of training, he was assigned to Tempelhof Central Airport, West Berlin, West Germany where he served as a Russian linguist. In 1983, he returned to Goodfellow AFB as a Russian linguist instructor. In May, 1985, Tom was selected to complete his Bachelor of Science degree in Electrical Engineering at Arizona State University, Tempe, AZ, under the Airmen Education and Commissioning Program. Upon graduation, Tom attended Officer Training School at Lackland AFB, TX and received his commission in April 1987. After a brief training tour at Keesler AFB, MS, he was assigned to Headquarters, Tactical Air Command, Langley AFB, VA where he managed embedded computer systems on the F-22, F-117A, F-16, and other high-payoff weapon systems. In May 1991, Tom entered the Air Force Institute of Technology, Wright-Patterson AFB, OH in pursuit of a Master of Science Degree in Electrical Engineering

Permanent address: 4145 Mathilda St.
        Pittsburgh, PA 15234

REPORT DOCUMENTATION PAGE

Public reporting burden for this collection of information is estimated to average 1 hour per response, including the time for reviewing instructions, searching existing data sources, gathering and maintaining the data needed, and completing and reviewing the collection of information. Send comments regarding this burden estimate or any other aspect of this collection of information, including suggestions for reducing this burden, to Washington Headquarters Services, Directorate for Information Operations and Reports, 1215 Jefferson Davis Highway, Suite 1204, Arlington, VA 22202-4302, and to the Office of Management and Budget, Paperwork Reduction Project (0704-0188), Washington, DC 20503.

1. AGENCY USE ONLY (leave blank)	2. REPORT DATE December 1992	3. REPORT TYPE AND DATES COVERED Master's Thesis

4. TITLE AND SUBTITLE

SCIENTIFIC VISUALIZATION OF VOLUMETRIC
RADAR CROSS SECTION (RCS) DATA

5. FUNDING NUMBERS

6. AUTHOR(S)

Thomas G. Wojszynski, Capt, USAF

7. PERFORMING ORGANIZATION NAME(S) AND ADDRESS(ES)

Air Force Institute of Technology, WPAFB OH 45433-6583

8. PERFORMING ORGANIZATION REPORT NUMBER

AFIT/GCS/ENG/92D-21

9. SPONSORING / MONITORING AGENCY NAME(S) AND ADDRESS(ES)

Capt Kevin A. Cox
ESC/MP
Hanscom AFB, MA

10. SPONSORING / MONITORING AGENCY REPORT NUMBER

11. SUPPLEMENTARY NOTES

12a. DISTRIBUTION / AVAILABILITY STATEMENT

Approved for public release; distribution unlimited

12b. DISTRIBUTION CODE

13. ABSTRACT (Maximum 200 words)

For aircraft design and mission planning, designers, threat analysts, mission planners, and pilots require a Radar Cross Section (RCS) central tendency with its associated distribution about a specified aspect and its relation to a known threat. Historically, RCS data sets have been statically analyzed to evaluate a design or mission profile. However, Scientific Visualization, the application of computer graphics techniques to produce pictures of complex physical phenomena, appears to be a more promising tool to interpret this data. This work describes data reduction techniques and a surface rendering algorithm to construct and display a complex polyhedron from adjacent contours of RCS data. Data reduction is accomplished by sectorizing the data and characterizing the statistical properties of the data. Color, lighting, and orientation cues are added to complete the visualization system. The tool may be useful for synthesis, design, and analysis of complex, low observable air vehicles.

14. SUBJECT TERMS

Scientific Visualization, Radar Cross Section, Surface Extraction,
Object Modeling, Triangulation, Statistical Radar Cross Section, Low Observable

15. NUMBER OF PAGES

58

16. PRICE CODE

17. SECURITY CLASSIFICATION OF REPORT	18. SECURITY CLASSIFICATION OF THIS PAGE	19. SECURITY CLASSIFICATION OF ABSTRACT	20. LIMITATION OF ABSTRACT
Unclassified	Unclassified	Unclassified	UL

NSN 7540-01-280-5500